

SUSY-induced FCNC top-quark processes at the Large Hadron Collider

J. J. Cao¹, G. Eilam¹, M. Frank², K. Hikasa³, G. L. Liu⁴, I. Turan², J. M. Yang⁵

¹ *Physics Department, Technion, 32000 Haifa, Israel*

² *Department of Physics, Concordia University, Montreal, H4B 1R6, Canada*

³ *Department of Physics, Tohoku University, Sendai 980-8578, Japan*

⁴ *Service de Physique Theorique CP225, Universite Libre de Bruxelles, 1050 Brussels, Belgium*

⁵ *Institute of Theoretical Physics, Academia Sinica, Beijing 100080, China*

We systematically calculate various flavor-changing neutral-current top-quark processes induced by supersymmetry at the Large Hadron Collider, which include five decay modes and six production channels. To reveal the characteristics of these processes, we first compare the dependence of the rates for these channels on the relevant supersymmetric parameters, then we scan the whole parameter space to find their maximal rates, including all the direct and indirect current experimental constraints on the charm-stop flavor mixings. We find that, under all these constraints, only a few channels, through $cg \rightarrow t$ at parton-level and $t \rightarrow ch$, may be observable at the Large Hadron Collider.

PACS numbers: 14.80.Ly, 11.30.Hv

I. INTRODUCTION

The study of various flavor-changing neutral-current (FCNC) processes has been shown to be very useful. In particular, as the heaviest fermion in the standard model (SM), the top quark may play a special role in FCNC phenomenology. In the SM the FCNC interactions of the top quark are extremely suppressed by the GIM mechanism, so that no FCNC top quark rates can reach an observable level at current or future colliders [1–3]. Thus, the observation of any FCNC top quark process would be a robust evidence for new physics beyond the SM. Due to its heaviness, the top quark is very sensitive to new physics. Indeed, several models beyond the SM often predict much larger FCNC top quark interactions [4]. Such FCNC interactions can induce various top quark production and decay channels, which can be explored in future collider experiments [5, 6] and serve as a good probe for new physics.

So far, much effort has been spent on the exploration of the FCNC top quark interactions. On the experimental side, the Tevatron CDF and D0 collaborations have reported interesting bounds on the FCNC top quark decays from Run 1 experiment and will tighten the bounds from the ongoing Run 2 experiments [7]. On the theoretical side, various FCNC top quark decays and top-charm associated productions at high energy colliders were extensively studied in the SM [1–3], the Minimal Supersymmetric Standard Model (MSSM) [8–12] and other new physics models [13–15]. These studies showed that the SM predictions for such processes are far below the detectable level. However, some new physics can enhance them by several orders of magnitude, which makes them potentially accessible at future colliders.

The Large Hadron Collider (LHC) at CERN will be a powerful machine for studying the top quark properties such as its FCNC interactions since it will produce top quarks copiously. Analysis [5] showed that some FCNC top quark rare decays with branching ratios as low as $\mathcal{O}(10^{-5})$ could be accessible at the LHC. Due to its high energy and high luminosity, the LHC will be the main utility for exploring FCNC top quark production channels [5].

The minimal supersymmetric standard model (MSSM) is a leading candidate for new physics beyond the SM and its consequences will be extensively explored at the LHC. In this paper, we thoroughly investigate various top quark FCNC processes in the framework of the MSSM. A characteristic feature of the model is that, in addition to the FCNC interactions generated at loop level by the CKM mixing matrix in the SM, it predicts FCNC interactions from soft SUSY breaking terms [16]. These additional FCNC interactions depend on the squark flavor mixings, and for the case of top quark, they are sensitive to the potentially large mixings between charm squarks (scharms) and top squarks (stops).

In this paper, we will examine six production channels, which proceed through the parton-level:

$$gg \rightarrow t\bar{c}, \quad (1)$$

$$cg \rightarrow t, \quad (2)$$

$$cg \rightarrow tg, \quad (3)$$

$$cg \rightarrow tZ, \quad (4)$$

$$cg \rightarrow t\gamma, \quad (5)$$

$$cg \rightarrow th, \quad (6)$$

and five FCNC top quark decay modes:

$$t \rightarrow cg, \quad (7)$$

$$t \rightarrow cgg, \quad (8)$$

$$t \rightarrow cZ, \quad (9)$$

$$t \rightarrow c\gamma, \quad (10)$$

$$t \rightarrow ch, \quad (11)$$

Among these, the decays $t \rightarrow cg, cgg, cZ, c\gamma, ch$ and the production $gg \rightarrow t\bar{c}$ have already been studied in the MSSM before [8, 11, 12], while the others have not been studied so far. Here we perform a comprehensive study of all these processes in the MSSM for the following purposes:

- (1) Since in the MSSM all these processes are induced mainly by scharm-stop mixings and each of them involves the same set of SUSY parameters, they are correlated. Although some of them have been studied in the literature, they were treated individually in different papers. Even though a combined analysis has been done in [5] within the framework of effective Lagrangian where the coefficients of all FCNC interactions are independent, such analysis is missing in an explicit model. Therefore, a comprehensive and comparative study of all these processes in an explicit model is necessary.
- (2) Through a comparative study of all these channels, we could determine the relative size of their rates. This is useful since the LHC experiments can in principle measure each of them and the pattern of relative rates can be tested. Only by considering all these processes together, we might know which one has the largest rate and will hopefully be discovered at the LHC, if the MSSM is the correct framework.
- (3) By scrutinizing the dependence of the rates of these transitions on the relevant SUSY parameters, one can determine the most sensitive parameters of the model and then discuss how the future LHC measurements could possibly bound them.
- (4) Performing the scan over the whole parameter space, subject to all the direct and indirect current experimental constraints on the scharm-stop flavor mixings [17], the maximal rate for each process can be determined and, in this way, we can pinpoint which ones are hopefully observable at the LHC. Of course, this does not mean that one should give up searching for those low-rate processes at the LHC. As stated above, the LHC measurements can readily place bounds on the sensitive SUSY parameters and such bounds are complementary to the current experimental constraints, most of which are indirect constraints.

This paper is organized as follows. In Sec. II we discuss the possible sources of flavor violation in the MSSM and give the FCNC interaction Lagrangian relevant to our calculations. In Sec. III we introduce a method to calculate various top quark FCNC processes. This method, as will be shown, can greatly simplify our calculations. The predictions of the rates are given in Sec. IV, with emphasis on illustrating the characteristics of their dependence on the relevant SUSY parameters. In Sec. V we consider various experimental constraints on the sources of flavor violation and scan the parameter space to find the maximal rates at the LHC. We draw our conclusion in Sec. VI. Finally, we give the expressions for the loop results in the Appendix.

II. FCNC INTERACTIONS IN THE MSSM

There are two sources of flavor violation in the MSSM [16]. The first one arises from the flavor mixings of up-quarks and down-quarks, which are described by the CKM matrix (inherited from the SM). The second one results from the misalignment between the rotations that diagonalize the quark and squark sectors due to the presence of soft SUSY

breaking terms. This source can induce large top quark FCNC processes and is the focus of investigation in this paper.

In the super-CKM basis with states $(\tilde{u}_L, \tilde{c}_L, \tilde{t}_L, \tilde{u}_R, \tilde{c}_R, \tilde{t}_R)$ for up-squarks and $(\tilde{d}_L, \tilde{s}_L, \tilde{b}_L, \tilde{d}_R, \tilde{s}_R, \tilde{b}_R)$ for down-squarks, the 6×6 squark mass matrix \mathcal{M}_q^2 ($\tilde{q} = \tilde{u}, \tilde{d}$) takes the form [16]

$$\mathcal{M}_q^2 = \begin{pmatrix} (M_{\tilde{q}}^2)_{LL} + m_q^2 + \cos 2\beta M_Z^2 (T_3^q - Q_q s_W^2) \hat{1} & (M_{\tilde{q}}^2)_{LR} - m_q \mu (\tan \beta)^{-2T_3^q} \\ (M_{\tilde{q}}^2)_{LR}^\dagger - m_q \mu (\tan \beta)^{-2T_3^q} & (M_{\tilde{q}}^2)_{RR} + m_q^2 + \cos 2\beta M_Z^2 Q_q s_W^2 \hat{1} \end{pmatrix}, \quad (12)$$

where the soft mass parameters $(M_{\tilde{q}}^2)_{LL}$, $(M_{\tilde{q}}^2)_{LR}$ and $(M_{\tilde{q}}^2)_{RR}$ are 3×3 matrices in flavor space, $\hat{1}$ stands for the unit matrix, m_q is the diagonal quark mass matrix, $T_3^q = 1/2$ for up-squarks and $T_3^q = -1/2$ for down-squarks, and $\tan \beta = v_2/v_1$ is the ratio of the vacuum expectation values of the Higgs fields. In general, the soft mass parameters are flavor non-diagonal. Since the low energy experimental data, such as $K^0 - \bar{K}^0$, $D^0 - \bar{D}^0$ and $B_d^0 - \bar{B}_d^0$ mixings, require the flavor mixings involving the first generation squarks to be negligibly small [16], we only consider the flavor mixings of the second and third generations and parametrize the soft mass parameters as

$$\begin{aligned} (M_{\tilde{u}}^2)_{LL} &= \begin{pmatrix} M_{Q_1}^2 & 0 & 0 \\ 0 & M_{Q_2}^2 & \delta_{LL} M_{Q_2} M_{Q_3} \\ 0 & \delta_{LL} M_{Q_2} M_{Q_3} & M_{Q_3}^2 \end{pmatrix}, \\ (M_{\tilde{u}}^2)_{LR} &= \begin{pmatrix} 0 & 0 & 0 \\ 0 & 0 & \delta_{LR} M_{Q_2} M_{U_3} \\ 0 & \delta_{RL} M_{U_2} M_{Q_3} & m_t A_t \end{pmatrix}, \\ (M_{\tilde{u}}^2)_{RR} &= (M_{\tilde{u}}^2)_{LL} |_{M_{Q_i}^2 \rightarrow M_{U_i}^2, \delta_{LL} \rightarrow \delta_{RR}}, \end{aligned} \quad (13)$$

for up-type squarks. Similarly, for down-squarks we have

$$\begin{aligned} (M_{\tilde{d}}^2)_{LR} &= \begin{pmatrix} 0 & 0 & 0 \\ 0 & 0 & \delta_{LR}^d M_{Q_2} M_{D_3} \\ 0 & \delta_{RL}^d M_{D_2} M_{Q_3} & m_b A_b \end{pmatrix}, \\ (M_{\tilde{d}}^2)_{RR} &= (M_{\tilde{d}}^2)_{LL} |_{M_{Q_i}^2 \rightarrow M_{D_i}^2, \delta_{LL} \rightarrow \delta_{RR}^d}. \end{aligned} \quad (14)$$

Due to $SU_L(2)$ gauge invariance, $(M_{\tilde{d}}^2)_{LL}$ is given by

$$(M_{\tilde{d}}^2)_{LL} = V_{CKM}^\dagger (M_{\tilde{u}}^2)_{LL} V_{CKM}. \quad (15)$$

Note that the mixing parameters, δ^d in the down sector defined in Eq. (14) are independent of δ in the up sector defined in Eq. (13), and in general, $\delta_{LR} \neq \delta_{RL}$. For the diagonal elements of left-right mixings in Eq. (13) and Eq. (14), we only kept the terms of third-family squarks, since we adopted the popular assumption that they are proportional to the corresponding quark masses.

It is clear that the mixing parameters in the squark mass matrices affect both the squark mass and its interactions. For example, in the presence of flavor mixings, squark-quark interactions are given by

$$V(\bar{q} X \tilde{q}'_\alpha) = \Gamma_q^{i\alpha} V(\bar{q} X \tilde{q}'_i), \quad (16)$$

where $V(\bar{q} X \tilde{q}'_\alpha)$ denotes the interaction in squark mass-eigenstates, $V(\bar{q} X \tilde{q}'_i)$ is that in the interaction basis, X may be gluino, neutralino or chargino, and Γ_q is the unitary matrix which diagonalizes the squark mass matrix. For the convenience in the following discussions, we give the interaction Lagrangian for up-type quarks [16, 18]:

$$\mathcal{L}_{u\tilde{u}\tilde{g}} = \sum_{i=1}^3 \sqrt{2} g_s T_{st}^a \left[\bar{u}_i^s (\Gamma_U)^{i\alpha} P_L \tilde{g}^a \tilde{u}_\alpha^t - \bar{u}_i^s (\Gamma_U)^{(i+3)\alpha} P_R \tilde{g}^a \tilde{u}_\alpha^t + \text{h.c.} \right], \quad (17)$$

$$\begin{aligned} \mathcal{L}_{u\tilde{u}\tilde{\chi}^0} &= \sum_{n=1}^4 \sum_{i=1}^3 \frac{g}{\sqrt{2}} \left\{ \bar{u}_i N_{n1}^* \frac{4}{3} \tan \theta_W P_L \tilde{\chi}_n^0 (\Gamma_U)^{(i+3)\alpha} \tilde{u}_\alpha - \bar{u}_i N_{n4}^* \frac{(m_u)_{ij}}{M_W \sin \beta} P_L \tilde{\chi}_n^0 (\Gamma_U)^{j\alpha} \tilde{u}_\alpha \right. \\ &\quad \left. - \bar{u}_i \left(N_{n2} + \frac{1}{3} N_{n1} \tan \theta_W \right) P_R \tilde{\chi}_n^0 (\Gamma_U)^{i\alpha} \tilde{u}_\alpha - \bar{u}_i N_{n4} \frac{(m_u)_{ij}}{M_W \sin \beta} P_R \tilde{\chi}_n^0 (\Gamma_U)^{(j+3)\alpha} \tilde{u}_\alpha \right\}, \end{aligned} \quad (18)$$

$$\begin{aligned} \mathcal{L}_{u\tilde{d}\tilde{\chi}^\pm} &= \sum_{\sigma=1}^2 \sum_{i,j=1}^3 g \left\{ \bar{u}_i [V_{\sigma 2}^* \left(\frac{m_u}{\sqrt{2} M_W \sin \beta} V_{CKM} \right)_{ij}] P_L \tilde{\chi}_\sigma^\pm (\Gamma_D)^{j\alpha} \tilde{d}_\alpha - \bar{u}_i [U_{\sigma 1} (V_{CKM})_{ij}] P_R \tilde{\chi}_\sigma^\pm (\Gamma_D)^{j\alpha} \tilde{d}_\alpha \right. \\ &\quad \left. + \bar{u}_i [U_{\sigma 2} (V_{CKM} \frac{m_d}{\sqrt{2} M_W \cos \beta})_{ij}] P_R \tilde{\chi}_\sigma^\pm (\Gamma_D)^{(j+3)\alpha} \tilde{d}_\alpha \right\} + \text{h.c.}, \end{aligned} \quad (19)$$

where T^a are the $SU(3)_c$ generators, $i = 1, 2, 3$ is the generation index, $\alpha = 1, \dots, 6$ is the squark flavor index, s and t are color indices, N is the 4×4 rotation matrix defined by $N^* M_{\tilde{\chi}_0} N^{-1} = \text{diag}(m_{\tilde{\chi}_1^0}, m_{\tilde{\chi}_2^0}, m_{\tilde{\chi}_3^0}, m_{\tilde{\chi}_4^0})$, the index σ refers to chargino mass eigenstates, and V and U are the usual chargino rotation matrices defined by $U^* M_{\tilde{\chi}^\pm} V^{-1} = \text{diag}(m_{\tilde{\chi}_1^\pm}, m_{\tilde{\chi}_2^\pm})$. From the above interactions one can see that FCNC neutralino and gluino interactions only arise from up-type squark mixings, while the FCNC chargino interactions are induced from both the off-diagonal elements in the CKM matrix, and from the flavor mixings in down-type squark mass matrix.

Although each of the above interactions contributes to the top quark FCNC transitions by gaugino mediated loops, the contributions could be of quite different magnitude. Since both the neutralino and gluino contributions depend on the same parameters in the up-type squark mass matrix, their different coupling strength indicate that the neutralino contribution is much smaller than the gluino contribution, except for a very massive gluino and light neutralino scenario. Noting that B-physics requires small $\delta^d \leq \mathcal{O}(0.1)$ [19–21], the FCNC interactions induced by charginos are in general not large. Recently, these three types of contributions to $gg \rightarrow t\bar{c}$ at the LHC were simultaneously calculated in [12], and it was shown that both the neutralino and the chargino contribution are several orders of magnitude smaller than the gluino contribution for most SUSY parameter space. Since we are mostly interested in the parameter regions with large predictions for FCNC processes, in this paper we consider only the gluino-mediated contributions.

Even if only the gluino-mediated loops are considered in calculating the top quark FCNC interactions, the model has still a large parameter set. Beside the gluino mass, there are nine soft mass parameters in the scharm-stop mass matrix, which complicates our analysis. In order to simplify our calculations, we neglect the charm quark mass. Then the amplitude squared for any top quark FCNC mode/channel considered in this paper can be decomposed as

$$|M|^2 = |M|_L^2 + |M|_R^2, \quad (20)$$

where $|M|_L^2$ ($|M|_R^2$) is the amplitude squared with a left-handed (right-handed) charm quark, as either an external state or internal state in Feynman diagrams. Furthermore, by using the mass insertion method[22], one can easily find that $|M|_L^2$ ($|M|_R^2$) vanishes if there is no left-handed (right-handed) scharm mixings with stop, and that these amplitudes have a weaker dependence on right-handed (left-handed) scharm mixings than on the left-handed (right-handed) scharm mixings. These features, verified numerically by our calculations, motivate us to consider the case with only left-handed scharm mixings in top quark FCNC processes. In this case, the relevant soft mass parameters are reduced to seven, since we set $\delta_{RL}\delta_{RR} = 0$ and $M_{U_2}^2$ is irrelevant to our calculation (see Eq. (13)). Throughout this paper, we always consider this case, but we note that for those transitions not involving W, Z bosons, the results for $|M|_L^2$ can be applied to $|M|_R^2$ with the substitutions $R \leftrightarrow L$ and $M_{U_i} \leftrightarrow M_{Q_i}$.

Another reason for considering only left-handed scharm mixings with stops is that these are well motivated in popular flavor-blind SUSY breaking scenarios, such as the mSUGRA model [23] and gauge-mediated SUSY-breaking models [24]. In these models, the sfermion-mass matrices are flavor diagonal at the SUSY-breaking scale, but the Yukawa couplings can induce flavor mixings when evolving the matrices down to the electroweak scale. Estimates of these radiatively induced off-diagonal squark-mass terms indicate the magnitude for left-handed flavor mixings are proportional to bottom quark mass, while those for the right-handed scharm are proportional to charm quark mass [25]. Therefore, in phenomenological studies of scharm-stop mixings, one usually assumes the existence of left-handed scharm mixings.

Finally, it should be pointed out that although we make use of the parametrization in Eqs.(12-14), which is widely used in the literature for the calculations by mass insertion approximation, our calculations are the full computation in the mass eigensate basis of squarks (that is we first diagonalize the squark mass matrices and then perform the loop calculations in the mass eigensate basis). Such a treatment, unlike the mass insertion method [22] which makes sense only for $\delta's < 1$, can allow for $\delta's > 1$ (as will be shown in Sec. V, in some cases $\delta's > 1$ can be permitted by all experimental constraints because we use non-universal squark mass parameters, that is M_Q, M_U and M_D are not degenerate). Note that although all our numerical results are obtained from such full computation in the mass eigenstate basis, we will utilize the mass insertion method when we try to qualitatively explain the behaviors of some results.

III. THE EFFECTIVE VERTEX METHOD

We introduce a method which can greatly simplify our calculations since it avoids repetition of the evaluation of a same loop-corrected vertex in different places, or in different processes. All results in this paper were obtained by this method, and some of them were cross-checked by other tools such as `FormCalc` [26].

The key point of our method is the so-called ‘‘effective vertex’’. To illustrate this method we consider $gg \rightarrow t\bar{c}$ as an example. The Feynman diagrams for this process are shown in Fig. 1. The SUSY-QCD contributions to the

$c - t$ transition and the vertex $\bar{t}c\bar{g}$, as well as the box diagrams, are given in Fig. 2. Noting that the amplitude for Fig. 1(a) can be split into two terms, one containing a charm quark propagator, and the other containing a top quark propagator

$$M_a \propto \frac{i}{\not{q} - m_t} i\Sigma(q) \frac{i}{\not{q} - m_c} = \frac{i(\not{q} + m_t)}{m_c^2 - m_t^2} i\Sigma(q) \frac{i}{\not{q} - m_c} + \frac{i}{\not{q} - m_t} i\Sigma(q) \frac{i(\not{q} + m_c)}{m_t^2 - m_c^2}, \quad (21)$$

we collect the first term together with Fig. 1(e, f), and combine the second term together with Fig. 1(g, h). After this arrangement, we can define a momentum dependent effective $\bar{t}c\bar{g}$ interaction as

$$\Gamma_\mu^{eff}(p_t, p_c) = \Gamma_\mu^{\bar{t}c\bar{g}}(p_t, p_c) + i\Sigma(p_t) \frac{i(\not{p}_t' + m_c)}{m_t^2 - m_c^2} \Gamma_\mu^{\bar{q}qg} + \Gamma_\mu^{\bar{q}qg} \frac{i(\not{p}_c' + m_t)}{m_c^2 - m_t^2} i\Sigma(p_c), \quad (22)$$

where $\Gamma_\mu^{\bar{t}c\bar{g}}$ is the penguin diagram contribution to the effective interaction and $\Gamma_\mu^{\bar{q}qg}$ is the usual QCD vertex. Then the calculation of Fig. 1(a-h) is equivalent to the calculation of the “tree” level transition depicted in Fig. 3(a-c), which obviously has a simpler structure. By following this method, our calculations can be greatly simplified, since the effective $\bar{t}c\bar{g}$ interaction appears in many processes, and the effective $\bar{t}c\bar{g}$ interaction is the same for all channels considered in the paper.

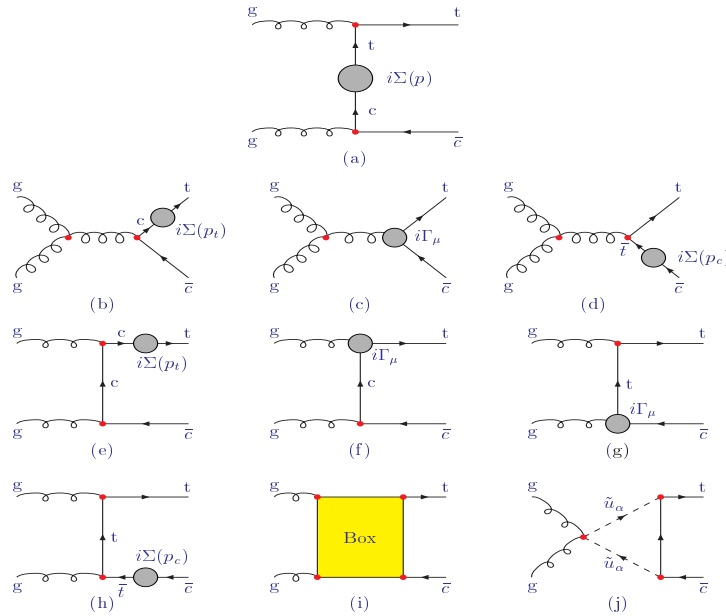


FIG. 1: Feynman diagrams for $gg \rightarrow t\bar{c}$. Additional diagrams with the two gluons interchanged are not shown.

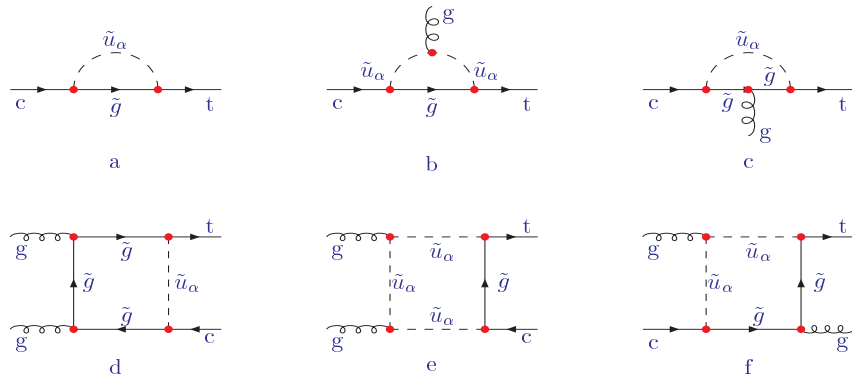


FIG. 2: SUSY-QCD contribution to $c - t$ transition, $\bar{t}c\bar{g}$ interaction and box diagrams for $gg \rightarrow t\bar{c}$.

Of course, the effective vertex $\bar{t}c\bar{g}$ is model-dependent since its components $\Gamma_\mu^{\bar{t}c\bar{g}}$ and Σ are model-dependent. We obtained their expressions in SUSY QCD analytically. We retain the tensor loop functions rather than expanding

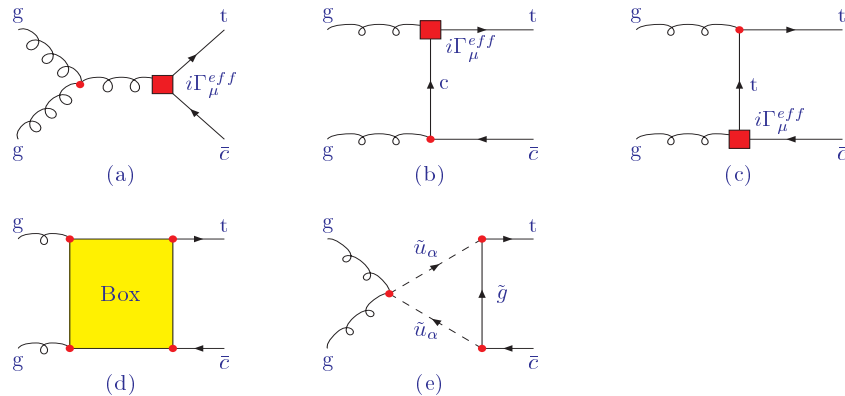


FIG. 3: Effective diagrams for the process $gg \rightarrow t\bar{c}$. Here Γ_μ^{eff} is the effective $\bar{t}cg$ interaction defined in Eq. (22).

them in terms of scalar loop functions as usual [27]. This method makes our results quite compact and also simplifies our Fortran codes which will be discussed below.

The effective vertex $\bar{t}cg$ in Eq. (22) is a 4-component Lorentz vector and also a 4×4 matrix in Dirac spinor space. In its realization in Fortran coding, we use a dimension-three array $V(i, j, k)$ with i ($=1,2,3,4$) labeling the Lorentz index and j, k ($=1,2,3,4$) labeling the spinor indices. We also use arrays to encode other quantities such as Lorentz vectors, Dirac spinors, Lorentz tensors and Dirac γ matrices. The steps to calculate the effective interaction in Fortran code can be then summarized as follows:

- Input the matrices $P_{L,R}$, $\gamma^\mu P_{L,R}$ and $\sigma^{\mu\nu}$. For any other matrices encountered in the calculation, we use γ algebra to generate its elements.
- Use the mass splitting method[28] to generate events with momenta for the initial and final particles.
- For a generated event with fixed momenta, the components of any tensor loop function can be calculated numerically and stored in arrays.
- Generate the γ matrices $\gamma^{\mu_1} \dots \gamma^{\mu_n}$ and contract its Lorentz indices with those of tensor loop functions and those of quark momenta to obtain the effective vertex.

To calculate the amplitude of $gg \rightarrow t\bar{c}$, we also need to calculate box diagrams. Such calculations are usually tedious if the four-point tensor loop functions are expanded in terms of scalar loop functions. Since we choose to retain the tensor loop functions and contract the indices numerically, our results are quite compact, as shown for $gg \rightarrow t\bar{c}$ in the Appendix. The general expression for a box diagram is the sum of fermion chain of the form $(\bar{u}\gamma^{\mu_1} \dots \gamma^{\mu_n} u) \times D_{\mu_i \dots \mu_j} \times p_{\mu_k} \dots$ and its numerical value is calculated by the following steps

- Input the wave functions for fermions and define the multiplication of γ matrix with the wave function.
- Generate the tensor, say $\bar{u} \dots \gamma^{\mu_{n-1}} \gamma^{\mu_n} u$, and contract its indices with those of loop functions $D_{\mu_i \dots \mu_j}$ and those of vectors involved, to get the value of each term in the amplitude.

With the method introduced above, we can also easily calculate other FCNC interactions. Let us take the calculation of $cg \rightarrow tZ$ as an example. Its Feynman diagrams can be obtained from Figs. 1-2 by removing those involving triple-gluon interaction and gluon-gluino-gluino interaction, and then replacing any gluon with Z boson. Using the technique from Eq. (21) to introduce the effective $\bar{t}cg$ interaction and the effective $\bar{t}cZ$ interaction, one can again get simplified diagrams similar to Fig. 3(b-e).

Once $gg \rightarrow t\bar{c}$ is calculated, evaluation of the others $t \rightarrow cg$, $cg \rightarrow tg$ and $t \rightarrow cgg$ becomes rather easy. The decay $t \rightarrow cg$ is now a tree level interaction induced by the interaction $\bar{t}cg$. The amplitudes (or their conjugates) for $cg \rightarrow tg$ and $t \rightarrow cgg$ are related to that of $gg \rightarrow t\bar{c}$, and can be easily obtained by making some simple replacements which can be easily realized in our code.

In the Appendix, we list the explicit forms of all the penguin-induced FCNC interactions discussed in this paper. These interactions are needed to obtain the effective top FCNC interactions.

IV. NUMERICAL RESULTS AND DEPENDENCE ON SUSY PARAMETERS

We know, from the discussion in Section II, that the calculations of the SUSY-QCD contributions induced by the flavor mixings between left-handed scharm and stop, depend on the parameters $M_{Q_{2,3}}$, M_{U_3} , $X_t = A_t - \mu \cot \beta$, $m_{\tilde{g}}$, δ_{LL} and δ_{LR} . In this section, we investigate the dependence of the numerical results on these parameters. We first show the results for top quark rare decays. These decay modes occur only via one effective interaction and thus their dependence on the parameters is relatively simple. We perform a comparative study and plot the results for these decays together, to illustrate their dependence on a given set of parameters. After analyzing the features of the top quark rare decays, we extend the study to the FCNC top quark productions. They usually involve two effective interactions and several box diagrams, and thus their dependence on SUSY parameters is more complex.

The SM parameters used in our calculations are [29]

$$\begin{aligned} m_t &= 172.7 \text{ GeV}, & m_b &= 4.8 \text{ GeV}, & m_Z &= 91.19 \text{ GeV}, \\ \sin \theta_W &= 0.2228, & \alpha_s(m_t) &= 0.1095, & \alpha &= 1/128. \end{aligned} \quad (23)$$

After the assumptions discussed in Sec. III, about 10 SUSY parameters are still involved. We will show below the dependence on SUSY parameters of the top FCNC processes. When one of the parameters is varied, the others will be fixed to their ‘‘central’’ values, taken as

$$M_{\text{SUSY}} = M_{Q_3} = M_{U_3} = M_{Q_2} = 500 \text{ GeV}, \quad X_t = 1000 \text{ GeV}, \quad m_{\tilde{g}} = 250 \text{ GeV}, \quad \tan \beta = 5. \quad (24)$$

The values of δ_{LL} and δ_{LR} will be shown in the figures. With the exception of the last plot in this section (Fig. 12), we adopt the so-called m_h^{max} scenario [30] which is widely discussed in Higgs physics, and which assumes that all the soft mass parameters are degenerate

$$M_{\text{SUSY}} = M_{Q_i} = M_{U_i} = M_{D_i}, \quad (25)$$

and that all the trilinear couplings are also degenerate, $A_{u_i} = A_{d_i}$, with $X_t/M_{\text{SUSY}} = 2$. In investigating the processes $t \rightarrow ch$ and $cg \rightarrow th$, we used the loop-corrected lightest Higgs boson mass and the effective Higgs mixing angle [17, 31]. These two quantities involve two additional parameters μ and m_A , which are fixed as

$$\mu = m_A = 500 \text{ GeV}. \quad (26)$$

In our calculations we use CTEQ6L [32] to generate the parton distributions with renormalization scale μ_R and factorization scale μ_F , chosen to be $\mu_R = \mu_F = m_t$. To make our predictions more realistic, we applied some kinematic cuts. For example, for the three body decay $t \rightarrow cgg$ we require that the energy of each decay product be larger than 15 GeV and the separation of any two final states be more than 15° in the top quark rest frame. For the top quark production channels, we require that the transverse momentum of each produced particle be larger than 15 GeV and their pseudo rapidity be less than 2.5 in the laboratory frame. Moreover, for $cg \rightarrow t$ followed by $t \rightarrow bW$, we do not require the top quark exactly on mass shell and instead we require the invariant mass of bottom quark and W boson in a region of $m_t - 3\Gamma_t \leq M_{bW} \leq m_t + 3\Gamma_t$ (Γ_t is the top quark width). This requirement was once used in [33] to investigate the observability of this channel at hadron colliders in the effective Lagrangian framework.

Furthermore, we vary the flavor mixings, δ_{LL} and δ_{LR} , over a wide range, with the only requirement that they satisfy current collider searches for sparticles and Higgs bosons [29]:

$$m_{\tilde{q}} \geq 96 \text{ GeV}, \quad m_{\tilde{g}} \geq 195 \text{ GeV}, \quad m_h \geq 85 \text{ GeV}. \quad (27)$$

In principle, some low energy data, such as $b - s$ transition and $\delta\rho$, can also constrain these mixings [17]. But those so-called indirect constraints are usually quite complicated. To simplify the discussion in this section we do not impose these indirect constraints, but we address such a question in the next section. We checked that the conclusions obtained in this section are valid in the region favored by these indirect constraints [60].

In Figs. 4-6, we present the branching ratios of various FCNC top quark decays, defined with respect to the width $\Gamma_t(t \rightarrow bW)$ ($\simeq 1.45 \text{ GeV}$). We plot the six branching ratios for the decays in Eq. (7)-(11) as functions of $m_{\tilde{g}}$, M_{SUSY} and X_t in the upper two diagrams of Fig. 4, the lower two diagrams of Fig. 4 and Fig. 5, respectively. We also show the dependence of the branching ratios on the squark mixing parameter δ_{LL} (δ_{LR}) by fixing the value of δ_{LR} (δ_{LL}) in Fig. 6. These figures show some common features of all the gauge boson decay modes. The first one is that, as the sparticles become heavy, the branching ratios drops monotonously (see Fig. 4), a reflection of the decoupling property of the MSSM. The second is that, as shown in Fig. 5, the branching ratios increase with the increase of X_t . This is because X_t affects the squark mass splittings and could alleviate the cancellation between different loop contributions. The third feature is that the branching ratios increase rapidly with the flavor mixing δ_{LL} and δ_{LR} ,

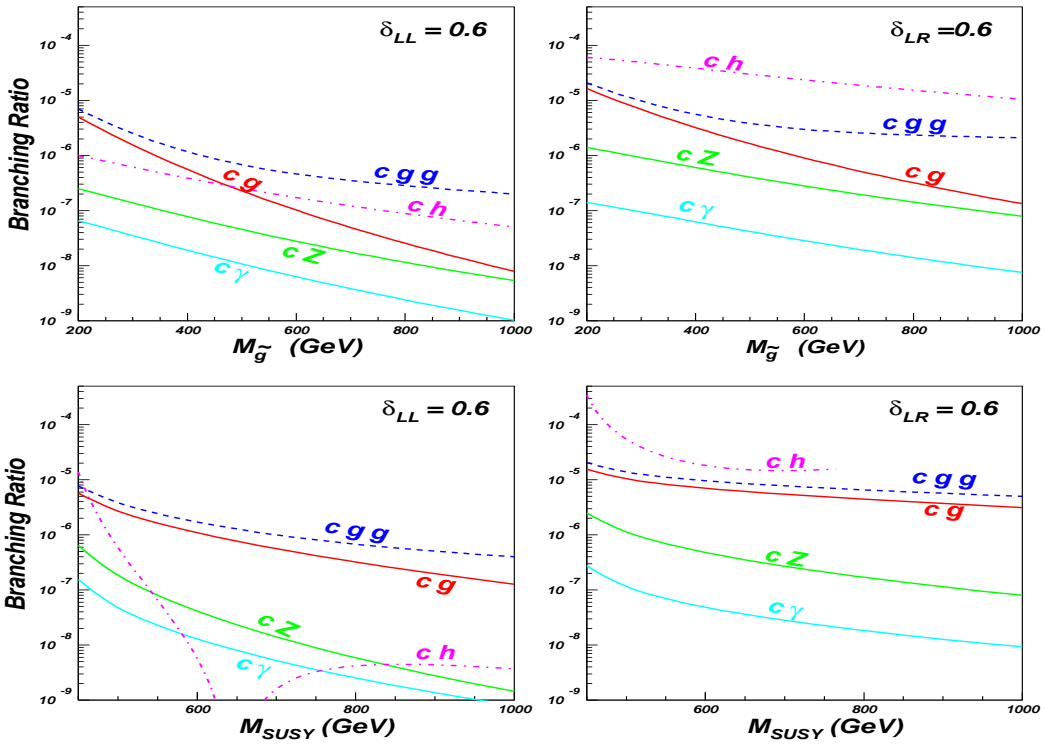


FIG. 4: The branching ratios of FCNC top quark decays. Unspecified parameters are given in Eqs. (23-26). The values of δ_{LL} and δ_{LR} are arbitrarily chosen, and a smaller value will lower the rates, but not change the tendencies of these curves.

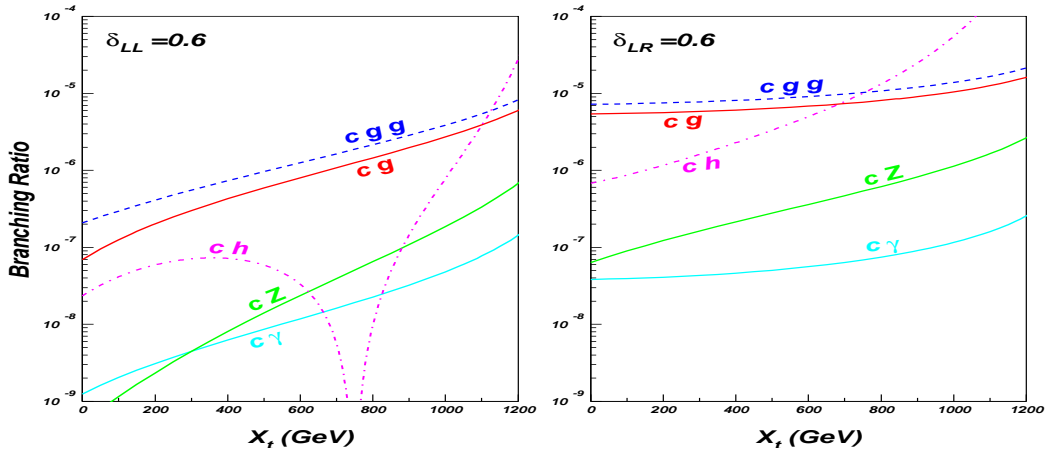


FIG. 5: Same as Fig. 4, but as functions of $X_t (= A_t - \mu \cot \beta)$.

because the flavor mixings can not only enhance the coupling strength of squark flavor changing interactions, but also enlarge the squark mass splittings. This is illustrated in the first two diagrams of Fig. 6. These last two effects combined make the branching ratios very sensitive to the flavor mixing parameters.

By comparing the case $\delta_{LL} \neq 0$ with the case $\delta_{LR} \neq 0$ throughout Figs. 4-6, one finds that δ_{LR} induces larger rates with weaker dependence on sparticle masses. Furthermore, when both δ_{LL} and δ_{LR} are non-zero, as can be inferred from the last two diagrams of Fig. 6, the δ_{LL} and the δ_{LR} dependences interfere destructively. To understand such behaviors, we resort to the mass insertion method, as it can give more intuitive results [22]. We take the decay $t \rightarrow cg$

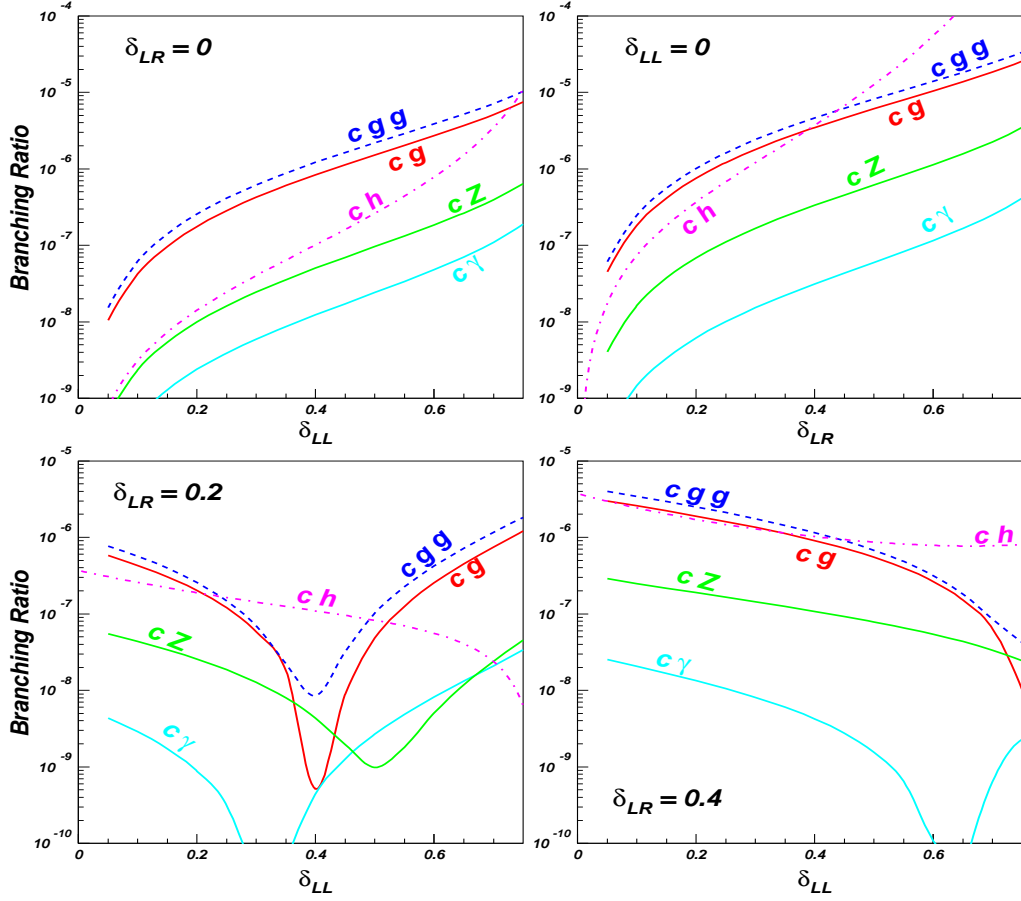


FIG. 6: Same as Fig. 4, but as functions of the mixing parameters.

as an example. By gauge invariance, the general expression for the effective $\bar{t}cg$ interaction takes the form

$$\Gamma_\mu = F_1(k^2)\bar{t}T^a(k^2\gamma_\mu - k_\mu \not{k})P_Lcg^a - m_tF_2(k^2)\bar{t}T^a i\sigma_{\mu\nu}k^\nu P_Lcg^a \quad (28)$$

where $F_{1,2}(k^2)$ are form factors arising from loop calculations. For the decay $t \rightarrow cg$, F_1 does not contribute, since the gluon momentum k^μ satisfies $k^2 = 0$ and $k \cdot \epsilon = 0$. So only the dipole moment term is relevant to our discussion. Noting that the dipole changes both the flavor and the chirality of the fermions, we may infer the form of m_tF_2 in the mass insertion approximation. If only δ_{LL} is considered for flavor changing, m_tF_2 must be

$$m_tF_2 = \frac{m_t\delta_{LL}}{M_{SUSY}^2}A + \frac{m_{\tilde{g}}\delta_{LL}m_tX_t}{M_{SUSY}^4}B, \quad (29)$$

where $M_{SUSY} = \max(m_{\tilde{g}}, M_{\tilde{q}})$, and A, B are dimensionless constants coming from loop functions with $1/M_{SUSY}^2$ factored out. The first term corresponds to the top chirality flipping contribution, i.e., obtained by using the relation $\bar{u}_t \not{y}_t = m_t \bar{u}_t$, while the second term corresponds to the $\tilde{t}_L - \tilde{t}_R$ mixing contribution, and thus associated with the gluino mass. The situation is quite different for $\delta_{LR} \neq 0$, which alone can be responsible for both flavor changing and chirality flipping. In this case, m_tF_2 should be

$$m_tF_2 = \frac{m_{\tilde{g}}\delta_{LR}}{M_{SUSY}^2}C. \quad (30)$$

where C , like A and B , is a dimensionless constant coming from loop functions with $1/M_{SUSY}^2$ factored out. Comparing Eq. (29) with Eq. (30), we find that the latter is larger if $m_{\tilde{g}} \gg m_t$. Assuming that $m_{\tilde{g}} \simeq M_{\tilde{q}}$, Eq. (29) scales like $1/M_{SUSY}^2$ while Eq. (30) scales like $1/M_{SUSY}$. This explains the fact that δ_{LR} induces larger rates with weaker dependence on sparticle masses. Moreover, a detailed calculation shows that m_tF_2 in Eq. (29) is of opposite sign to that in Eq. (30), which means that the δ_{LL} contribution tends to cancel the δ_{LR} contribution.

The decay $t \rightarrow ch$ has similar features to the decay into a gauge boson except for a rather complicated dependence on M_{SUSY} and X_t , as shown in Figs. 4-5. For the effective $t\bar{c}h$ interaction, with both the top and the charm quarks on-shell, the general expression is

$$\Gamma_{t\bar{c}h}^{eff} = D\bar{t}P_Lch, \quad (31)$$

where D is a form factor emanating from the loop calculation. This interaction, like the effective $\bar{t}cg$ interaction, also involves both flavor change and chirality flip. So in some aspects, the behavior for $t \rightarrow ch$ should be similar to $t \rightarrow cg$. But its dependence on X_t is more complicated than other decay modes. The reason may be that X_t not only affects the masses and mixings of squarks, but also affects the Higgs boson mass and its mixing angles, and, further, it enters the interaction of $\tilde{q}^*\tilde{q}h$.

An interesting feature, shown in Figs. 4-6 is that the branching ratio of $t \rightarrow cg$ is always smaller than the higher order decay $t \rightarrow cgg$. This was observed in the SM [2] and the MSSM [12], and it indicates that the QCD corrections to $t \rightarrow cg$ may be important. Two reasons may account for this behavior. One is that the QCD factor in the amplitude-square for $t \rightarrow cgg$ is much larger than that for $t \rightarrow cg$. The other reason is that, unlike the case $t \rightarrow cg$, F_1 in Eq. (28) also contributes to $t \rightarrow cgg$ and this contribution is important. From Figs. 4-6, one finds that, in most cases

$$Br(t \rightarrow cgg) > Br(t \rightarrow cg) > Br(t \rightarrow cZ) > Br(t \rightarrow c\gamma), \quad (32)$$

and in some cases $Br(t \rightarrow ch)$ may be the largest.

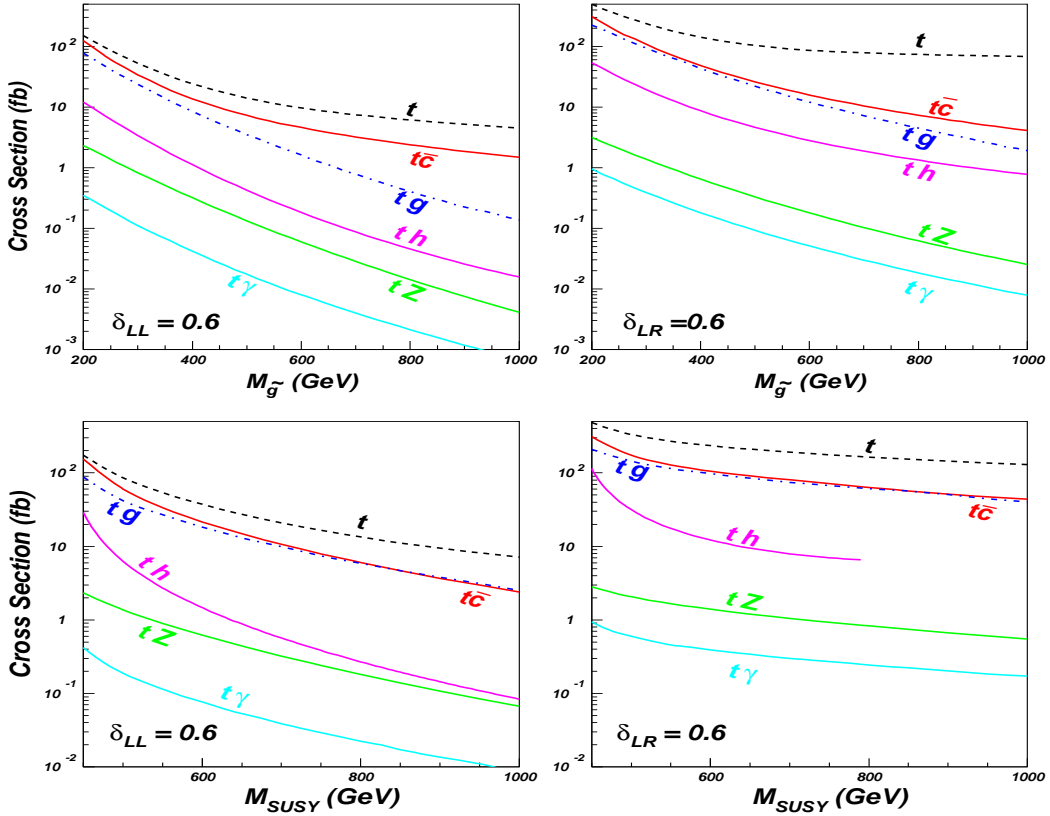


FIG. 7: The cross sections of the FCNC top quark productions at the LHC. Each curve labeled by the final states corresponds to a certain production channel.

After giving the branching ratios for the FCNC top decays comparatively, we now consider the FCNC top quark production channels. At the LHC the production proceeds through the six parton-level processes shown in Eqs. (1-6), among which only $gg \rightarrow t\bar{c}$ has been extensively studied in the MSSM[11, 12]. In calculating the cross section for each channel, we also include the rate for its charge conjugate channel. In the following discussions we use the parton process to label its contribution to the hadronic one. Thus, the cross sections mentioned below refer to the hadronic ones.

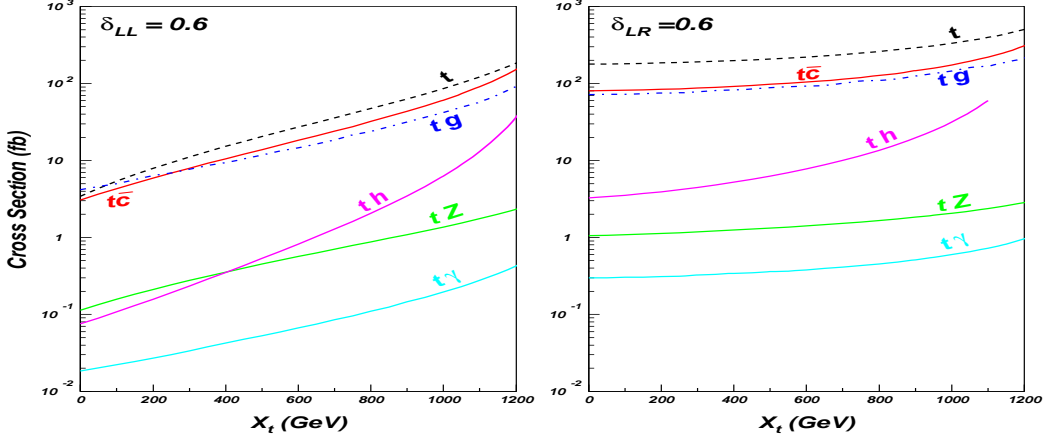


FIG. 8: Same as Fig. 7, but as a function of $X_t (= A_t - \mu \cot \beta)$.

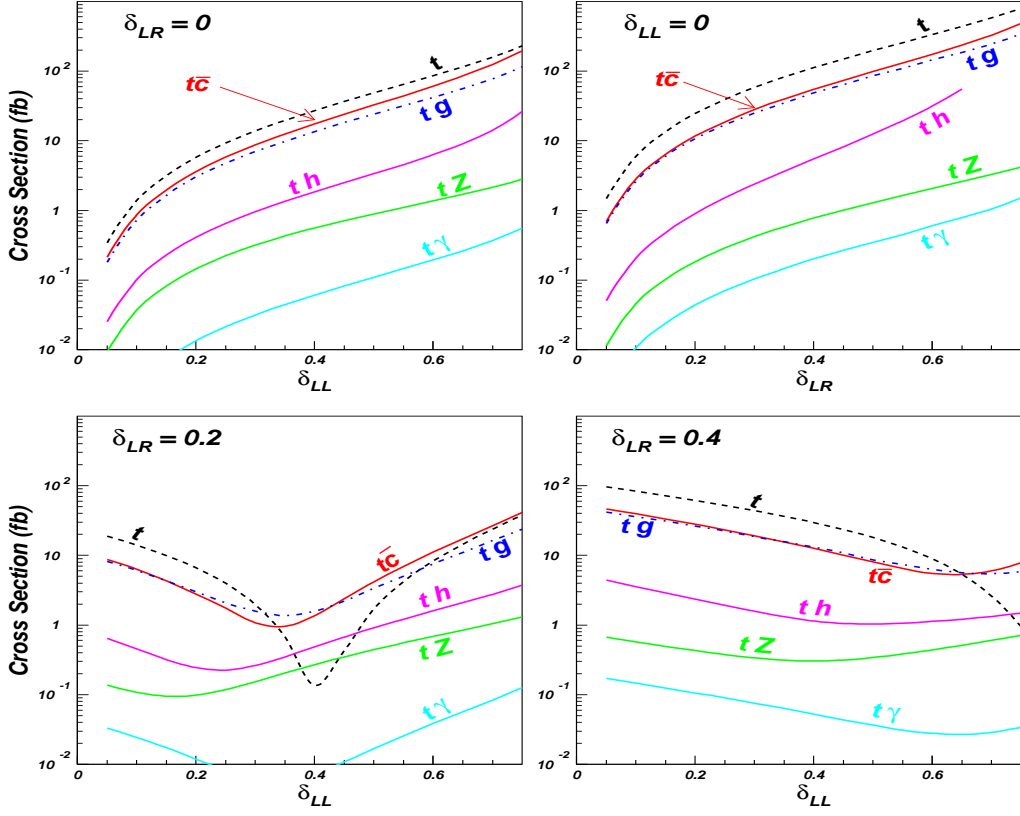


FIG. 9: Same as Fig. 7, but as a function of the mixing parameters.

The dependence of the cross sections on SUSY parameters is plotted in Figs. 7-9. These figures exhibit the same features as the FCNC top quark decays in Fig. 4-6. Thus we do not repeat drawing attention to the same features, and we only point out three remarkable points of these diagrams. The first is that the rate of $cg \rightarrow t$ is generally larger than that for $gg \rightarrow t\bar{c}$. This is possible because the charm quark in the parton distributions mainly comes from the splitting of a gluon [32] and thus $cg \rightarrow t$ can be seen as $gg \rightarrow t\bar{c}$ with the final charm quark going along the beam pipe. Analyzing the signal versus background [33, 34], it seems that $cg \rightarrow t$ provides a better opportunity for the observation of top production. The second point is that the rate of $cg \rightarrow tg$ is comparable to $gg \rightarrow t\bar{c}$ in most cases.

This coincides with the results in [35] where both modes were studied in the effective Lagrangian approach. Since the two processes have the same signals at colliders, namely single top plus one light-quark jet, one should combine these two when searching for the FCNC top production events. The third point is that in most cases the cross section for $cg \rightarrow th$ is one order of magnitude smaller than that for $gg \rightarrow t\bar{c}$. The reason is that although $cg \rightarrow th$ can proceed either through $\bar{t}cg$ interaction or $\bar{t}ch$ interaction, the two interactions interfere destructively and thus the combined contributions are suppressed.

As shown above, in most of parameter space the rates are expected to be quite small at the LHC. In order to study the observability of such rare processes, it is necessary to scan the whole parameter space to figure out the maximum value that each process can reach. We call the ‘favorable region’ the part of parameter space which gives the maximum value for the rate of an individual channel. Of course, such favorable region is process-dependent. In what follows we take $gg \rightarrow t\bar{c}$ as an example to carry out such a parameter scan explicitly. In the next section, the maximal rates for all processes will be tabulated, after discussing the effects of the indirect constraints on the flavor mixing parameters.

In Fig. 10 we plot the maximal cross section for $gg \rightarrow t\bar{c}$ as a function of X_t with non-zero δ_{LL} (left panel) and δ_{LR} (right panel). The maximum value is obtained by fixing M_{SUSY} and X_t but varying $m_{\tilde{g}}$ and δ_{LL} or δ_{LR} . In searching for such maximal values, we required $m_{\tilde{q}} \geq 100$ GeV and $m_{\tilde{g}} \geq 200$ GeV.

For non-zero δ_{LL} , we find that the parameter points for the maximal cross sections correspond to the lightest squark mass and the gluino mass fixed at their allowed lower bound, i.e., 100 GeV and 200 GeV, respectively. This can be easily understood from the decoupling property of the MSSM. At such optimum points, if M_{SUSY} is fixed, X_t value is related to δ_{LL} . Since both X_t and δ_{LL} are the off-diagonal elements in squark mass matrix, a large X_t will correspond to a small δ_{LL} and vice versa. Then from Eq. (29), one can see that neither large nor small X_t can predict the largest rate for $gg \rightarrow t\bar{c}$. This explains the behavior of each curve in the left panel of Fig. 10.

In Fig. 11, we plot the maximal cross section as a function of mixing parameters. For non-zero δ_{LL} mixings (left panel), we see that the maximal value of each curve lies at a moderate δ_{LL} , which agrees with the above analysis. Among the three curves for different M_{SUSY} , the maximal value is obtained for $M_{SUSY} = 800$ GeV. The reason is that $M_{SUSY} = 800$ GeV implies heavier masses for the other two squarks and alleviates the cancellation between different diagram contributions.

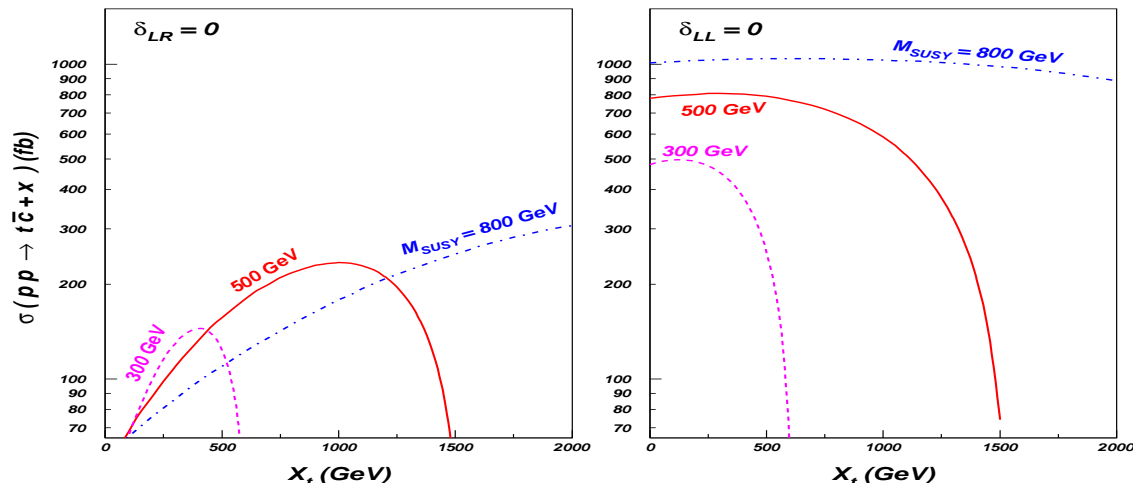


FIG. 10: The maximal cross section of $t\bar{c}$ production at the LHC, proceeding through the parton-level channel $gg \rightarrow t\bar{c}$, as a function of X_t by varying $m_{\tilde{g}}$ and δ_{LL} or δ_{LR} .

For the case of non-zero δ_{LR} , maximal cross sections also appear at the lower bounds of the lightest squark mass and the gluino mass. This property together with the effective $\bar{t}cg$ coupling in Eq. (30), imply that the maximal value for each curve should lie at a large δ_{LR} , or by the correlation, at small X_t . (Both X_t and δ_{LR} appear as the off-diagonal elements in squark mass matrix. Thus, for a given M_{SUSY} , their large values enlarge the mass splitting between squark mass eigenstates and lead to a small mass for the lightest squark. Due to the lower bound on the lightest squark mass, δ_{LR} and X_t cannot be both large.) This is in agreement with the behaviors of the curves for non-zero δ_{LR} shown in the right panels of Figs. 10-11. For the right panel of Fig. 10, we checked that for $M_{SUSY} = 800$ GeV, varying X_t from 0 to 500 GeV only resulted in a change of 0.006 for δ_{LR} . This is the reason that the maximal cross section is insensitive to X_t for $X_t \leq 500$ GeV.

In Fig. 12 we show the dependence of the maximal cross section on M_{SUSY} for non-zero δ_{LL} or δ_{LR} values. To

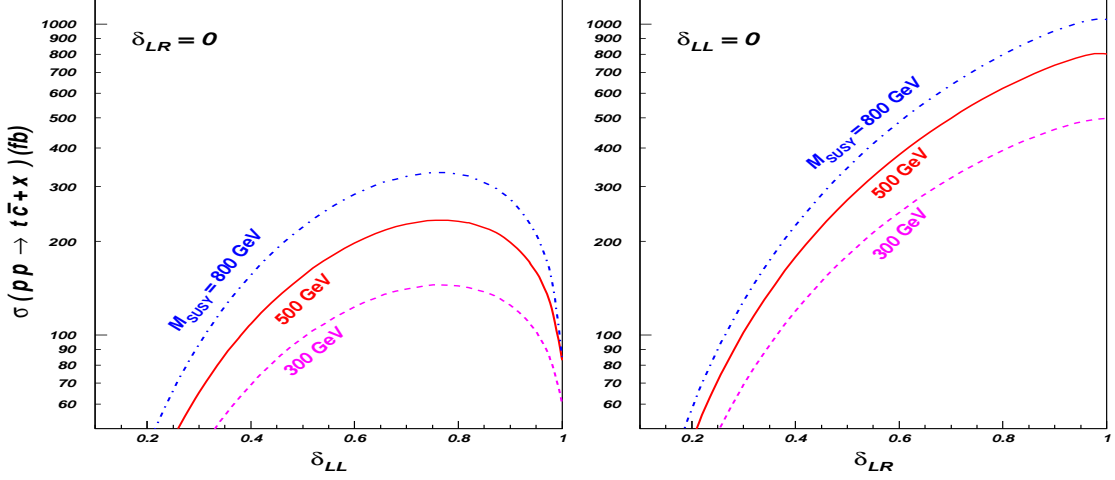


FIG. 11: Same as Fig. 10, but as a function of mixing parameters.

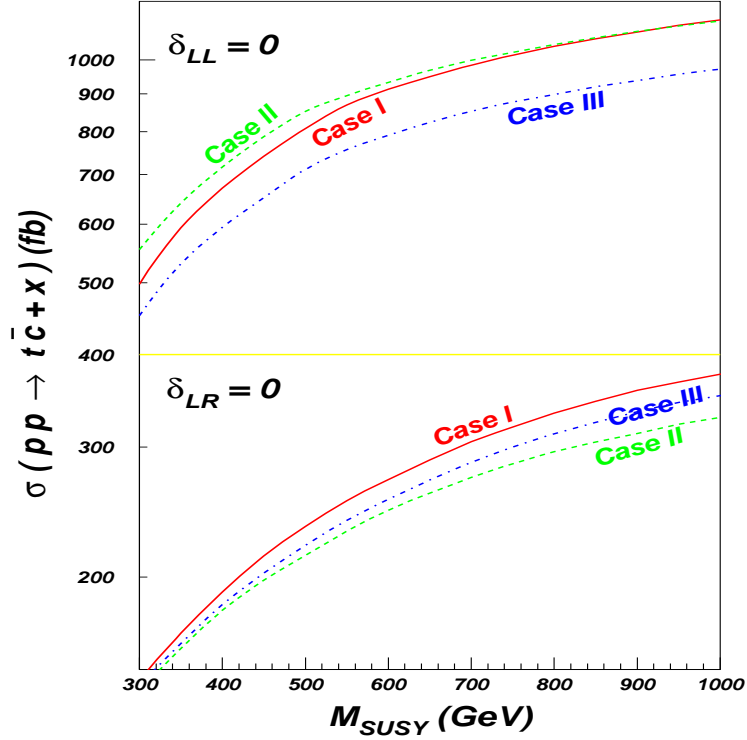


FIG. 12: Same as Fig. 10, but as a function of M_{SUSY} under different cases specified in the text.

get the maximal cross sections, we fix the lightest squark mass as 100 GeV and vary the value of δ_{LL} or δ_{LR} . We considered three cases,

- Case I: $M_{Q_2} = M_{Q_3} = M_{U_3} = M_{SUSY}$,
- Case II: $M_{Q_3} = M_{U_3} = M_{SUSY}$, $M_{Q_2} = 1.2M_{SUSY}$,
- Case III: $M_{Q_3} = M_{SUSY}$, $M_{U_3} = 0.8M_{SUSY}$, $M_{Q_2} = 1.2M_{SUSY}$.

These cases are motivated by mSUGRA model [23] where the three squark masses are generated from the same soft breaking mass parameter m_0 at supersymmetry breaking scale, but are split due to quark Yukawa couplings when

they evolve down to electroweak scale [36]. From this figure we see that the maximal cross section values increases with M_{SUSY} , and for non-zero δ_{LL} (δ_{LR}), case I (II) gives the largest prediction for the cross sections. These results indicate that in searching for the maximum values of the cross section, we should treat M_{Q_2} , M_{Q_3} and M_{U_3} as free parameters and explore all the possibilities for these masses.

Note that in the above discussions we have only considered the case for non-zero δ_{LL} or δ_{LR} . But as pointed below Eq. (20), most of our conclusions should be valid for the case non-zero δ_{RL} or $\delta_{RR} \neq 0$ with an interchange of L and R .

V. LOW-ENERGY CONSTRAINTS ON FCNC TOP QUARK INTERACTIONS

A. Constraints on scharm-stop flavor mixings

We know, from the discussions in the preceding section, that the rates of the FCNC top quark processes depend strongly on the flavor mixing parameters δ_{LL} and δ_{LR} , which are treated as free. Of course, such a treatment is informative and useful to the LHC experiments since it allows to directly place limits on the mixing parameters once the measurements are made at the LHC.

However, it is worth noting that these mixing parameters may be subject to various direct and indirect experimental constraints. Firstly, since the mixing terms appear as the non-diagonal elements of squark mass matrices, they can affect the squark mass spectrum, especially by enlarging the mass splitting between squarks. Therefore they should be constrained by the squark mass bounds from the direct experimental searches. At the same time, since the squark loops affect the precision electroweak quantities such as M_W and the effective weak mixing angle $\sin^2 \theta_{eff}$ [31, 37], such mixings could also be constrained by precision electroweak measurements. As shown in [17, 31], to a good approximation, the supersymmetric corrections to the electroweak quantities contribute through the $\delta\rho$ parameter and thus sensitive to the mass splitting of squarks. Secondly, the processes governed by $b \rightarrow s$ transition like $B_s - \bar{B}_s$ mixings [20] and $b \rightarrow s\gamma$ [19] can provide rich information about the $\tilde{s} - \tilde{b}$ mixings. Through the SU(2) relation between the up-squark and down-squark mass matrices (see Eq. (15)) and also through the electroweak quantities (since all squarks contribute to electroweak quantities via loops), the information can be reflected in the up-squark sector and hence constrain the scharm-stop mixings. Thirdly, we note that the chiral flipping mixings of scharm-stop come from the trilinear $H_2 \tilde{c}_L^* \tilde{t}_R$ interactions [16]. Such interactions can lower the lightest Higgs boson mass m_h via squark loops and thus should be subject to the current experimental bound on m_h .

In [17] these constraints were examined and it was shown that, although they usually depend on additional unknown parameters in the down-type squark mass matrix, a combined analysis can still severely restrict the mixings δ_{LL} and δ_{LR} in most cases. Here we extend the analysis of [17] by providing more examples about these constraints and then perform a detailed investigation of the maximum rates for various top quark FCNC processes both with and without these constraints.

The constraints considered in our paper are $b \rightarrow s\gamma$, $B_s - \bar{B}_s$ mixing, δM_W and $\delta \sin^2 \theta_{eff}$ and the lightest Higgs boson mass. In the following, we first recapitulate these constraints and then apply them to scharm-stop mixings.

- (1) $b \rightarrow s\gamma$: In the MSSM, there are four kinds of loops contributing to $b \rightarrow s\gamma$ mediated respectively by the charged Higgs bosons, charginos, neutralinos and gluinos, each of which may be sizable [19]. For a light charged Higgs mass, the contribution from the charged Higgs is quite large and always has the same sign as the SM contribution, and thus enhance the branching ratio to very high values [38]. The current $b \rightarrow s\gamma$ data require either a sufficiently heavy charged Higgs boson, or its contribution should be canceled by other parts of SUSY effects. For the other three kinds of contributions, depending on SUSY parameters, they may interfere constructively or destructively with the SM effects and thus their relative sizes are not fixed [39]. The effect of these properties of SUSY on $b \rightarrow s\gamma$ makes it necessary to consider all the contributions simultaneously in discussing $b \rightarrow s\gamma$ constraints on the squark flavor mixing parameters.

Current measurement of the branching ratio for $b \rightarrow s\gamma$ is rather precise, with 3σ bounds given by [40]

$$2.53 \times 10^{-4} < Br(b \rightarrow s\gamma) < 4.34 \times 10^{-4}. \quad (33)$$

With the SM prediction $Br^{NLO}(b \rightarrow s\gamma) = (3.53 \pm 0.30) \times 10^{-4}$ [41] and a favored negative C_7 by $b \rightarrow sl^+l^-$ [42], where C_7 denotes the Wilson coefficient for the electromagnetic dipole operator \mathcal{O}_7 , this decay can severely restrict the SUSY parameters. Our numerical results indicate that it is very sensitive to δ_{LR}^d and δ_{RL}^d for most cases, and for large $\tan\beta$, it is sensitive to δ_{LL} as well. The same results also indicate that $b \rightarrow s\gamma$ depends weakly on δ_{LR} which affects the decay via chargino-mediated loops, but under all circumstances $b \rightarrow s\gamma$ is not sensitive to δ_{RL} and δ_{RR} .

- (2) $B_s - \bar{B}_s$ mixing: In the MSSM, although the loops mediated by charged Higgs boson, chargino and neutralino contribute to $B_s - \bar{B}_s$ mixing, their effects are generally much smaller than the SM contribution[20]. So when discussing the constraint of $B_s - \bar{B}_s$ mixing on squark flavor mixing parameters, we only consider gluino contributions. Recently, the D0 collaboration gave the first two-side bound on the mass splitting between B_s and \bar{B}_s [43]

$$17 \text{ ps}^{-1} < \Delta M_s < 21 \text{ ps}^{-1} \quad (90\% \text{ C.L.}) \quad (34)$$

This result is in agreement with the SM prediction, which is estimated as $21.3 \pm 2.6 \text{ ps}^{-1}$ by the UTfit group [44] and $20.9_{-4.2}^{+4.5} \text{ ps}^{-1}$ by the CKMfitter group [45]. After considering various uncertainties, the bounds in Eq. (34) can be re-expressed as[46]

$$0.55 < |1 + M_{12}^{SUSY}/M_{12}^{SM}| < 1.37, \quad (35)$$

where M_{12} is the transition matrix element for $B_s - \bar{B}_s$ transition. As pointed out in[20], $B_s - \bar{B}_s$ mixing is very sensitive to the combinations $\delta_{LL}\delta_{RR}^d$ and $\delta_{LR}^d\delta_{RL}^d$ and thus can put rather stringent constraints on any of δ^d s.

- (3) δM_W and $\delta \sin^2 \theta_{eff}$: In the MSSM, the corrections to M_W and $\sin^2 \theta_{eff}$ involve the calculation of the gauge boson self energy, and among all kinds of contribution to the self energy, those from squark loops are most important[47]. As a good approximation, δM_W and $\delta \sin^2 \theta_{eff}$ are related to $\delta \rho$ by[31]

$$\begin{aligned} \delta M_W &\simeq \frac{M_W}{2} \frac{c_W^2}{c_W^2 - s_W^2} \delta \rho, \\ \delta \sin^2 \theta_{eff} &\simeq -\frac{c_W^2 s_W^2}{c_W^2 - s_W^2} \delta \rho, \end{aligned} \quad (36)$$

where

$$\delta \rho \equiv \frac{\Sigma_Z(0)}{M_Z^2} - \frac{\Sigma_W(0)}{M_W^2}. \quad (37)$$

Since the couplings are stronger for left-handed squarks than for right-handed squarks, $\delta \rho$ is sensitive to the mass splittings between left-handed up-squarks and down-squarks [47]. As far as δ_{LL} is concerned, due to the $SU(2)$ relation in Eq. (15), it changes up-squark and down-squark mass spectra simultaneously and thus its effects on $\delta \rho$ are generally small even for large δ_{LL} . For δ_{LR} and δ_{RL} , they are independent of δ_{LR}^d and δ_{RL}^d , which are very small as required by $b - s$ transition [19-21]. Thus a large δ_{LR} or δ_{RL} can induce a sizable mismatch between up-squark and down-squark mass spectra. As a result, large δ_{LR} or δ_{RL} can significantly change $\delta \rho$ [17].

With the recent analysis of the LEP data, the uncertainties in measuring M_W and $\sin^2 \theta_{eff}$ were significantly lowered to read [48]

$$\delta M_W < 34 \text{ MeV}, \quad \delta \sin^2 \theta_{eff} < 15 \times 10^{-5}. \quad (38)$$

These uncertainties imply that the new physics influence on $\delta \rho$ should be lower than 5.5×10^{-4} .

- (4) *Higgs boson mass* m_h : In the MSSM the loop-corrected lightest Higgs boson mass m_h is defined as the pole of the corrected propagator matrix, which can be obtained by solving the equation [49]

$$\left[p^2 - m_{h,tree}^2 + \hat{\Sigma}_{hh}(p^2) \right] \left[p^2 - m_{H,tree}^2 + \hat{\Sigma}_{HH}(p^2) \right] - \left[\hat{\Sigma}_{hH}(p^2) \right]^2 = 0, \quad (39)$$

where $m_{h,tree}$ and $m_{H,tree}$ are the tree-level masses of the neutral Higgs bosons h and H , and $\hat{\Sigma}_i(p^2)$ ($i = hh, hH, HH$) are the renormalized Higgs boson self energies. Among all SUSY contributions to the Higgs boson self energies, those from top and stop loops are by far dominant because of the large top quark Yukawa couplings[50]. In the presence of the flavor mixings in the up-squark mass matrix, stops will mix with other squarks, and in this case, the dominant contribution comes from the up-squark sector [31, 51].

Our results indicate that the Higgs boson mass is more sensitive to δ_{LR} than to δ_{LL} . The reason is that δ_{LL} affects the Higgs boson mass only by changing the squark interaction through the unitary matrix Γ in Eq. (16) while δ_{LR} can also appear directly in the coupling of trilinear $H_2 \tilde{c}_L \tilde{t}_R$ interaction, since the $\delta_{LR} M_{Q_2} M_{U_3}$ term

in up-squark mass matrix comes from this trilinear interaction, and this can reduce the lightest Higgs boson mass. Current collider searches for a MSSM Higgs boson have given the lower bounds on m_h in five benchmark scenarios in Higgs physics[52]. In our calculation, we use the limit

$$m_h > \begin{cases} 92.8 \text{ GeV} & \text{for } m_h^{max} \text{ scenario} \\ 85 \text{ GeV} & \text{for other scenarios} \end{cases} \quad (40)$$

As the first example of these constraints, we consider the m_h^{max} scenario with the parameters given in Eqs. (24,26). To determine these constraints, we also need to specify the values of the parameters in the down-squark mass matrix and the gaugino mass M_2 . In Fig. 13 we show the allowed region in $\delta_{LL} - \delta_{LR}$ plane for the parameters

$$\begin{aligned} M_S = M_{Q_i} = M_{U_i} = M_{D_i} = 500 \text{ GeV}, \quad X_t = 1000 \text{ GeV}, \quad M_{\tilde{g}} = 250 \text{ GeV}, \quad \tan\beta = 5, \\ \mu = M_A = M_2 = 500 \text{ GeV}, \quad \delta_{RL} = \delta_{RR} = 0, \quad \delta_{LR}^d = \delta_{RR}^d = \delta_{RL}^d = 0. \end{aligned} \quad (41)$$

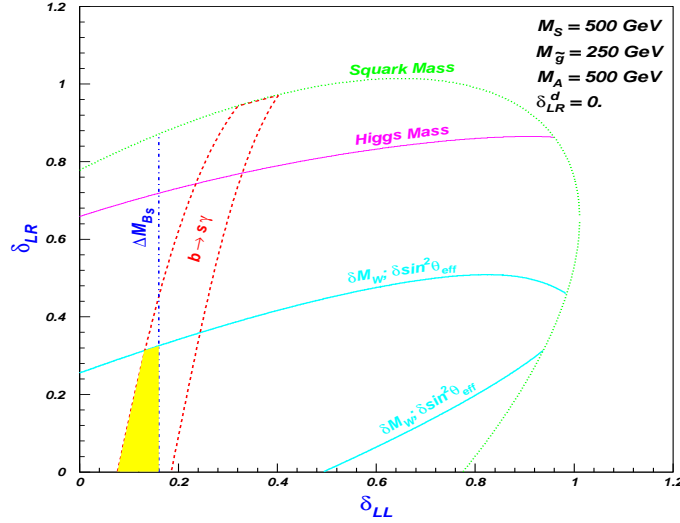


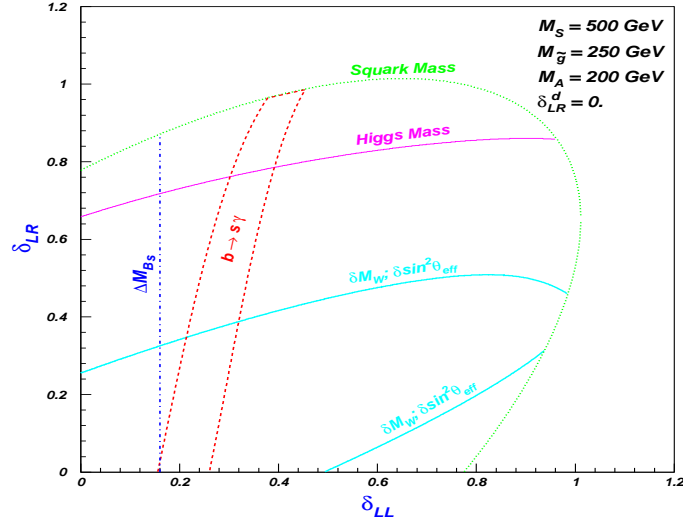
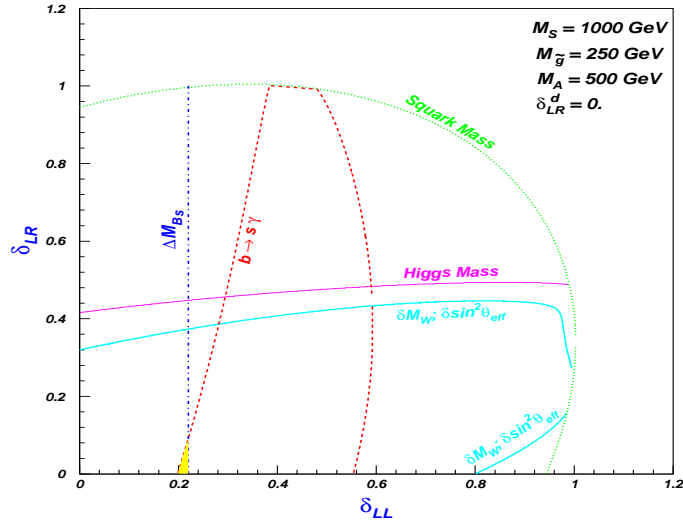
FIG. 13: Experimental constraints on δ_{LL} versus δ_{LR} with the parameters given in Eq. (41). The region under or left to each curve corresponds to the allowed region. The dashed-line enclosed area is allowed by $b \rightarrow s\gamma$. The colored area is the overlap region satisfying all the constraints.

Each curve in this figure corresponds to an experimental bound from Eqs. (27), (33), (35), (38) and (40); while the colored area is the overlap region satisfying all the constraints. The distinctive character of this figure is that $b \rightarrow s\gamma$ requires a non-zero δ_{LL} . The reason is that with the fixed parameters in Eq. (41), especially with $\delta_{LR}^d = 0$, the charged Higgs contribution enhances the SM contribution and, as a result, a non-zero gluino contribution is needed to cancel such effects. From Fig. 13 we see that the allowed region is mainly determined by $b \rightarrow s\gamma$ and $B_s - \bar{B}_s$ mixing. To show the dependence of such allowed region on SUSY parameters, we vary the values of M_A , M_S , $M_{\tilde{g}}$ and δ_{LR}^d one at a time, and get the allowed region (colored area) in Figs. 14, 15, 16 and 17, respectively. Explicitly, Fig. 14 corresponds to the parameters in Eq. (41) but with $M_A = 200 \text{ GeV}$, Fig. 15 corresponds to the parameters in Eq. (41) but with $M_S = 1000 \text{ GeV}$, and Fig. 16 and Fig. 17 are drawn in a similar way. The shift of the allowed region can be well understood by the properties of each constraint. Take Fig. 14 as an example. As M_A becomes smaller, the charged Higgs contribution to $b \rightarrow s\gamma$ further enhance the SM contribution and consequently a larger δ_{LL} is needed to cancel such effect and satisfy the bound in Eq. (33). Since the constraint from $B_s - \bar{B}_s$ mixing is not changed, the overlap region diminishes gradually and finally vanishes for $M_A \simeq 200 \text{ GeV}$.

As the second example, we consider the following parameters as an input

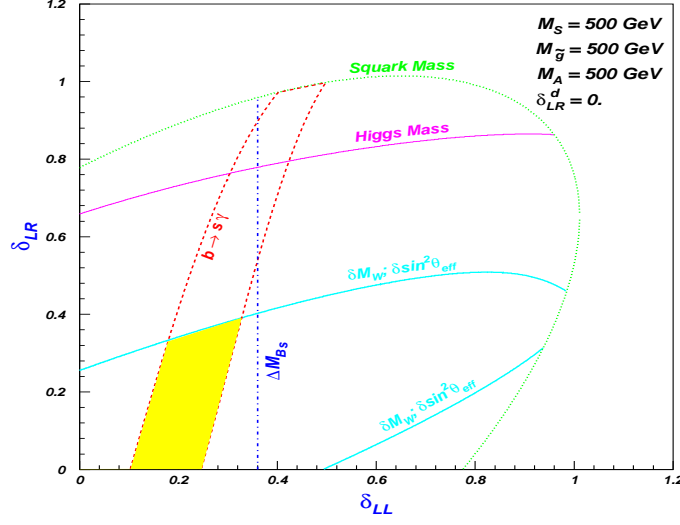
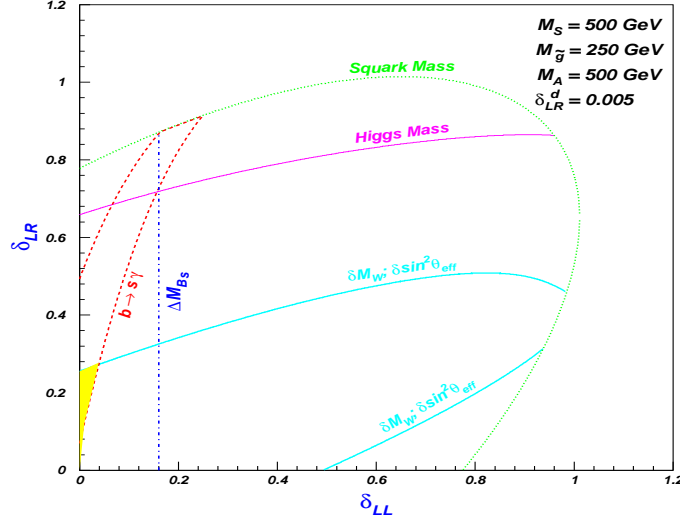
$$\begin{aligned} M_{Q_2} = 400 \text{ GeV}, \quad M_{Q_3} = 1000 \text{ GeV}, \quad M_{U_3} = 120 \text{ GeV}, \quad M_{\tilde{g}} = 196 \text{ GeV}, \quad M_A = 160 \text{ GeV}, \\ X_t = 33 \text{ GeV}, \quad \mu = -330 \text{ GeV}, \quad M_2 = 860 \text{ GeV}, \quad M_{D_i} = M_{Q_1} = M_{D_1} = 500 \text{ GeV}, \\ \delta_{LR}^d = 0.0026, \quad \delta_{RL} = \delta_{LR} = 0, \quad \delta_{RL}^d = \delta_{RR}^d = 0. \end{aligned} \quad (42)$$

This set corresponds to a point in the parameter space where $cg \rightarrow t$ is maximized for non-zero δ_{LR} (see following discussion about Table 1 and Table 2) and the results are depicted in Fig. 18. Since the squark masses are not universal,

FIG. 14: Same as Fig. 13, but for $M_A = 200$ GeV.FIG. 15: Same as Fig. 13, but for $M_S = 1$ TeV.

$\delta_{LR} > 1$ can still satisfy all the constraints and thus is allowed. The reason for this is that all the constraints actually limit the size of the product $\delta_{LR} M_{Q_2} M_{U_3}$. For the case discussed here, M_{Q_2} and M_{U_3} are not large and thus a large δ_{LR} is allowed.

A common property of the above several figures is that $B_s - \bar{B}_s$ mixing and $b \rightarrow s\gamma$ require a small δ_{LL} value. This is a general feature, which accounts for the significant suppression of the maximal predictions for various top quark FCNC interactions after considering all the constraints (see the results in case I ($\delta_{LR} = 0$) of Table 1). We also considered the constraints on δ_{RL} and δ_{RR} , which, as we pointed out earlier in this section, do not significantly affect $b \rightarrow s\gamma$ and $B_s - \bar{B}_s$ mixing, and hence are constrained only by $\delta\rho$ and the Higgs boson mass. We found that by comparing with the constraints on δ_{LR} and δ_{LL} , the constraints on these two mixing parameters, especially on δ_{RR} , are rather weak. Let us consider parameters in Eq. (41) as an example. For $\delta_{LL} = \delta_{LR} = 0$, our results indicate that δ_{RR} and δ_{RL} should be less than 0.76 and 0.46, respectively. Such constraints come from δM_W and $\delta \sin^2 \theta_{eff}$, and are sensitive to X_t . For $X_t = 0$, the bounds will be relaxed to 0.98 for δ_{RR} and 0.75 for δ_{RL} .

FIG. 16: Same as Fig. 13, but for $M_{\tilde{g}} = 500$ GeV.FIG. 17: Same as Fig. 13, but for $\delta_{LR}^d = 0.005$.

B. Maximal predictions in MSSM for FCNC top quark processes

With the constraints discussed above, we perform a scan over the SUSY parameter space to search for the maximal predictions of the MSSM on various top quark FCNC processes. We consider two cases: (I) only $\delta_{LL} \neq 0$ and (II) only $\delta_{LR} \neq 0$. For each case, we require the parameters to vary in the following ranges [61]

$$\begin{aligned}
 2 < \tan\beta < 60, & & 0 < M_{Q_i, U_i, D_i} < 1 \text{ TeV}, \\
 94 \text{ GeV} < m_A < 1 \text{ TeV}, & & 195 \text{ GeV} < m_{\tilde{g}} < 1 \text{ TeV}, \\
 0 < \delta_{LL} \text{ or } \delta_{LR} < 2, & & -1 \text{ TeV} < \mu, M_2 < 1 \text{ TeV}, \\
 0 < \delta_{LR}^b < 0.1, & & -2 \text{ TeV} < A_{t,b} < 2 \text{ TeV}.
 \end{aligned} \tag{43}$$

To manifest the effect of the combined constraints on the maximal rates, we present two types of predictions: one by only requiring the squark, chargino and neutralino masses satisfy their current lower bounds

$$m_{\tilde{u}} > 96 \text{ GeV}, \quad m_{\tilde{d}} > 89 \text{ GeV}, \quad m_{\tilde{\chi}^0} > 46 \text{ GeV}, \quad m_{\tilde{\chi}^+} > 94 \text{ GeV}; \tag{44}$$

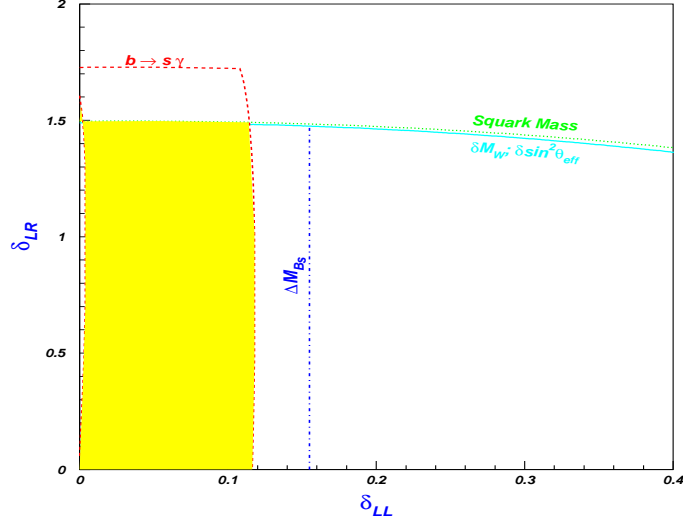


FIG. 18: Same as Fig. 13, but for the parameters in Eq. (42). In this case the Higgs boson mass cannot impose any constraints.

and the other by imposing all constraints in Eqs. (44, 33, 35, 38, 40). With five million samples for each process in either case, we obtain the maximal predictions and they are given in Table I. From the table one can see that the combined constraints can significantly decrease the MSSM predictions for top-quark FCNC channels at the LHC, especially for the case I, and among these FCNC processes, $cg \rightarrow th$ is the most affected one after imposing these constraints. The reason is that, as we pointed out before, there is a cancellation between the contribution from the effective interactions $\bar{t}cg$ and $\bar{t}ch$, and the constraints only allow a region with strong cancellation.

Table 1: Maximal predictions for top-quark FCNC processes induced by stop-scharm mixings via gluino-squark loops in the MSSM. For the production channels we show the hadronic cross sections at the LHC obtained from the given parton-level channels and the corresponding charge-conjugate channels. For the decays we show the branching ratios. LHC sensitivities listed in the last column are for 100fb^{-1} integrated luminosity.

	$\delta_{LL} \neq 0$		$\delta_{LR} \neq 0$		LHC sensitivity at 3σ level
	constraints masses	constraints all	constraints masses	constraints all	
$t \rightarrow ch$	1.2×10^{-3}	2.0×10^{-5}	2.5×10^{-2}	6.0×10^{-5}	5.8×10^{-5} [53]
$t \rightarrow cg$	5.0×10^{-5}	5.0×10^{-6}	1.3×10^{-4}	3.2×10^{-5}	—
$t \rightarrow cgg$	6.1×10^{-5}	7.1×10^{-6}	1.5×10^{-4}	3.5×10^{-5}	—
$t \rightarrow cZ$	5.0×10^{-6}	5.7×10^{-7}	1.2×10^{-5}	1.8×10^{-6}	3.6×10^{-5} [54, 55]
$t \rightarrow c\gamma$	9.0×10^{-7}	1.5×10^{-7}	1.3×10^{-6}	5.2×10^{-7}	1.2×10^{-5} [56, 59]
$cg \rightarrow t$	1450 fb	225 fb	3850 fb	950 fb	800 fb [33]
$gg \rightarrow t\bar{c}$	1400 fb	240 fb	2650 fb	700 fb	1500 fb [34, 35]
$cg \rightarrow tg$	800 fb	85 fb	1750 fb	520 fb	1500 fb [34, 35]
$cg \rightarrow t\gamma$	4 fb	0.4 fb	8 fb	1.8 fb	5 fb [57]
$cg \rightarrow tZ$	11 fb	1.5 fb	17 fb	5.7 fb	35 fb [57]
$cg \rightarrow th$	550 fb	18 fb	12000 fb	24 fb	200 fb [53]

Table 2: SUSY parameters leading to the maximal predictions for $\delta_{LR} \neq 0$ in Table 1.

process	$M_{Q_2}(GeV)$	$M_{Q_3}(GeV)$	$M_{U_3}(GeV)$	$X_t(GeV)$	$m_{\tilde{g}}(GeV)$	δ_{LR}
$t \rightarrow ch$	1000	900	225	500	195	1.1
$t \rightarrow cg$	310	985	90	100	195	1.72
$t \rightarrow cgg$	310	980	90	35	195	1.75
$t \rightarrow cZ$	500	900	165	600	198	1.1
$t \rightarrow c\gamma$	290	1000	90	20	196	1.72
$cg \rightarrow t$	400	990	120	33	196	1.5
$gg \rightarrow t\bar{c}$	310	990	85	80	196	1.8
$cg \rightarrow tg$	490	900	125	0	197	1.45
$cg \rightarrow t\gamma$	280	1000	85	25	197	1.78
$cg \rightarrow tZ$	370	920	80	115	196	1.86
$cg \rightarrow th$	280	1000	85	23	197	1.77

As one can see from Table 1, predictions for the case with non-zero δ_{LR} are larger than for the one with non-zero δ_{LL} . In Table 2 we list the SUSY parameters leading to the maximal predictions in Table 1 for the case II ($\delta_{LR} \neq 0$). It is seen from Table 2 that the ‘favorable’ parameters for the maximal rates are process dependent. Since these parameters could be first tested by seeking top quark FCNC signals at LHC, in Table 3 we present the predictions for all processes with two sets of parameters, called ‘Point 1’ and ‘Point 2’, where $t \rightarrow ch$ and $cg \rightarrow t$ are required to be maximized, respectively. It is seen that ‘Point 1’ favors $cg \rightarrow t$ as the production channel but ‘Point 2’ favors $t \rightarrow cgg$ among the decay modes.

Note that in Table 1 we only showed the cases of $\delta_{LL} \neq 0$ and $\delta_{LR} \neq 0$. For $\delta_{RL} \neq 0$, we found that the maximal rate of $t \rightarrow cg$ is 1.3×10^{-4} if only the squark mass constraints are included and 6×10^{-5} with all the constraints. For $\delta_{RR} \neq 0$, the maximal rate of $t \rightarrow cg$ is 5.0×10^{-5} with only the squark mass constraints and 4.85×10^{-5} with all the constraints. These results can be easily understood since, as discussed in [17] and in this section, the constraints on δ_{RL} and δ_{RR} are weaker than those for δ_{LR} and δ_{RR} , respectively.

Table 3: SUSY predictions for the rates of top quark FCNC processes at two points of parameter space: ‘Point 1’ maximizes $t \rightarrow ch$ and ‘Point 2’ maximizes $cg \rightarrow t$ channel.

process	Point 1	Point 2
$t \rightarrow cg$	2.0×10^{-5}	3.1×10^{-5}
$t \rightarrow cgg$	2.9×10^{-5}	3.5×10^{-5}
$t \rightarrow cZ$	1.4×10^{-6}	1.2×10^{-6}
$t \rightarrow c\gamma$	2.6×10^{-7}	5.2×10^{-7}
$t \rightarrow ch$	6.0×10^{-5}	7.0×10^{-9}
$cg \rightarrow t$	660 fb	950 fb
$gg \rightarrow t\bar{c}$	450 fb	690 fb
$cg \rightarrow tg$	280 fb	415 fb
$cg \rightarrow tZ$	2.3 fb	4.9 fb
$cg \rightarrow t\gamma$	1.2 fb	1.8 fb
$cg \rightarrow th$	24 fb	8.5 fb

C. Top FCNC observability at the LHC

Now we consider the observability of these top quark FCNC interactions at the LHC. This issue has been intensively investigated in the effective Lagrangian approach for $t \rightarrow ch$ [53], $t \rightarrow cZ$ [54, 55], $t \rightarrow c\gamma$ [56, 59], $pp \rightarrow t + X$ [33], $pp \rightarrow t\bar{c} + X$ [34, 35], $pp \rightarrow tg + X$ [34, 35], $pp \rightarrow tZ + X$ [57], $pp \rightarrow t\gamma + X$ [57] and $pp \rightarrow th + X$ [53]. At the LHC, most of the top quarks will be pair-produced. One of the tops is assumed to subsequently decay as $t \rightarrow bW$ (normal mode) while the other top goes to one of the above channels via FCNC interactions (exotic mode).

Due to the large QCD backgrounds at the LHC, the search for these processes must be performed in the decay channels $W \rightarrow \ell\bar{\nu}_\ell$ ($\ell = e, \mu$) for W boson, $Z \rightarrow \ell^+\ell^-$ for Z boson and $h \rightarrow b\bar{b}$ for Higgs boson. For any of these reactions, top quark reconstruction is required to extract the signal from its background. In Table 4, we list the signals and the main backgrounds. The detailed Monte Carlo simulations for the signals and backgrounds can be found in the corresponding literature listed in the last column of Table 1, where the LHC sensitivity for these processes is quoted. Although these sensitivities are based on the effective Lagrangian approach and may be not perfectly applicable to

the MSSM, we can take them as a rough criteria to estimate the observability of these channels. Comparing these sensitivities with the SUSY predictions, one can see that only the maximal predictions for $cg \rightarrow t$ and $t \rightarrow ch$ are slightly larger than the corresponding LHC sensitivities. This implies that the study of these processes may provide the first insight about top quark FCNC. From these sensitivities one can also see that, although the $gg \rightarrow t\bar{c}$ channel is now the most extensively studied among the FCNC production channels [11], its observation needs a higher luminosity. This is because $gg \rightarrow t\bar{c}$ has large irreducible backgrounds from single top productions in the SM [34]. Note that in Table 1, we did not list the sensitivity of the LHC to $t \rightarrow cg$, which has not been investigated because of a general belief that this decay is not well suited for detecting $\bar{t}cg$ interaction [5]. In fact, this decay was once investigated for the Tevatron [58], and it was found that due to the large background, namely W boson plus three jets, only a branching ratio as large as 5×10^{-3} may be accessible with 10 fb^{-1} integrated luminosity. This rate is about one order larger than that for $t \rightarrow c\gamma$ at the Tevatron with the same luminosity [59]. For the decay $t \rightarrow cgg$, there is an additional jet in its signal and its observability needs to be studied by a detailed Monte Carlo simulation.

Table 4: Experimental signature and main background for FCNC top rare decays and productions at the LHC. The top quarks are assumed to decay $t \rightarrow W^+b \rightarrow \ell^+\nu_\ell b$, and Z and h bosons decay in the channel $Z \rightarrow \ell^+\ell^-$ and $h \rightarrow b\bar{b}$, respectively.

Process	Signal	Background	Process	Signal	Background
$tt, t \rightarrow cg$	$jj\ell\nu b$	$Wjjj$	$cg \rightarrow t$	$\ell\nu b$	Wj
$tt, t \rightarrow cgg$	$jjj\ell\nu b$	$Wjjjj$	$gg \rightarrow t\bar{c}$	$\ell\nu bj$	tj
			$cg \rightarrow tg$	$\ell\nu bj$	tj
$tt, t \rightarrow cZ$	$\ell^+\ell^-j\ell\nu b$	$ZWjj$	$cg \rightarrow tZ$	$\ell^+\ell^-\ell\nu b$	ZWj
$tt, t \rightarrow c\gamma$	$\gamma j\ell\nu b$	γWjj	$cg \rightarrow t\gamma$	$\gamma\ell\nu b$	γWj
$tt, t \rightarrow ch$	$bbj\ell\nu b$	$Wbbjj$	$cg \rightarrow th$	$bb\ell\nu b$	tt

VI. CONCLUSIONS

In this paper, we investigated systematically the SUSY-induced top quark FCNC processes at the LHC, which includes various decay modes and production channels. We performed a comparative study for all the decay modes and for all the production channels so that one can see clearly which decay mode or production channel can have a relatively large rate. The dependence of these channels on the relevant SUSY parameters is investigated in detail and its properties are analyzed. We note that such a global study of the top quark FCNC processes has been done only in a model independent way [5]. We also analyzed the characteristics of the ‘favorable region’ in SUSY parameter space where the FCNC processes are maximized. After getting an understanding of these processes, we examined the effects of all the direct and indirect experimental constraints on the scharm-stop flavor mixings and scanned the parameter space to find their maximal rates with these constraints imposed. We found that $cg \rightarrow t$ and $t \rightarrow ch$ are the most likely channels to be observable at the LHC if the MSSM is the correct scenario beyond the SM.

Acknowledgment

This work is supported in part by a fellowship from the Lady Davis Foundation at the Technion, by the Israel Science Foundation (ISF), by NSERC of Canada under Grant No. SAP01105354, the National Natural Science Foundation of China under Grant No. 10475107 and 10505007, the Grant-in-Aid for Scientific Research (No. 14046201) from the Japan Ministry of Education, Culture, Sports, Science and Technology, and by the IISN and the Belgian science policy office (IAP V/27).

APPENDIX A: EXPRESSIONS FOR THE LOOP RESULTS

If significant flavor mixings exist only between left-handed scharm with stops, the squark states \tilde{c}_L , \tilde{t}_L and \tilde{t}_R will mix together to induce various top quark FCNCs. In this case, other squark states only serve as spectators to the processes considered in this paper. So in the actual calculation, we only need to consider the squark mass matrix for $(\tilde{t}_L, \tilde{t}_R, \tilde{c}_L)$, which is given by

$$\begin{pmatrix} M_{Q_3}^2 + m_t^2 + (\frac{1}{2} - \frac{2}{3}s_W^2)m_Z^2 \cos 2\beta & m_t(A_t - \mu \cot \beta) & \delta_{LL}M_{Q_2}M_{Q_3} \\ m_t(A_t - \mu \cot \beta) & M_{U_3}^2 + m_t^2 + \frac{2}{3}s_W^2 \cos 2\beta & \delta_{LR}M_{Q_2}M_{U_3} \\ \delta_{LL}M_{Q_2}M_{Q_3} & \delta_{LR}M_{Q_2}M_{U_3} & M_{Q_3}^2 + (\frac{1}{2} - \frac{2}{3}s_W^2)m_Z^2 \cos 2\beta \end{pmatrix}. \quad (\text{A1})$$

This mass matrix can be diagonalized by a unitary matrix V , and it enters the squark interactions as in Eq. (16).

In this Appendix, we list the expressions for Σ and $\Gamma_{\mu}^{\bar{t}cg}$ in Eq. (22) which are needed to get the effective $\bar{t}cg$ vertex. We also list the expressions for $\Gamma^{\bar{t}c\gamma}$, $\Gamma^{\bar{t}cZ}$ and $\Gamma^{\bar{t}ch}$ to calculate other effective vertices. Before presenting these expressions, we define the following abbreviations:

$$R^a = \sum_{\lambda=1}^3 V_{1\lambda} V_{\lambda 3}^{\dagger} B(p, m_{\bar{g}}, m_{\lambda}), \quad R^b = R^a|_{V_{1\lambda} \rightarrow V_{2\lambda}}, \quad (\text{A2})$$

$$R^c = \sum_{\lambda=1}^3 V_{1\lambda} V_{\lambda 3}^{\dagger} C(-p_c, p_c - p_t, m_{\bar{g}}, m_{\lambda}, m_{\lambda}), \quad R^d = R^c|_{V_{1\lambda} \rightarrow V_{2\lambda}}, \quad (\text{A3})$$

$$R^e = \sum_{\lambda=1}^3 V_{1\lambda} V_{\lambda 3}^{\dagger} C(-p_c, p_c - p_t, m_{\lambda}, m_{\bar{g}}, m_{\bar{g}}), \quad R^f = R^e|_{V_{1\lambda} \rightarrow V_{2\lambda}}, \quad (\text{A4})$$

$$R^g = \sum_{\lambda=1}^3 V_{1\lambda} V_{\lambda 3}^{\dagger} C(-p_b, p_b - p_t, m_{\bar{g}}, m_{\bar{b}_L}, m_{\lambda}), \quad (\text{A5})$$

$$R^h = \sum_{\rho, \lambda=1}^3 V_{1\lambda} F_{\lambda\rho}^Z V_{\rho 3}^{\dagger} C(-p_c, p_c - p_t, m_{\bar{g}}, m_{\rho}, m_{\lambda}), \quad R^i = R^h|_{V_{1\lambda} \rightarrow V_{2\lambda}}, \quad (\text{A6})$$

$$R^j = \sum_{\rho, \lambda=1}^3 V_{1\lambda} F_{\lambda\rho}^h V_{\rho 3}^{\dagger} C(-p_c, p_c - p_t, m_{\bar{g}}, m_{\rho}, m_{\lambda}), \quad R^k = R^j|_{V_{1\lambda} \rightarrow V_{2\lambda}}, \quad (\text{A7})$$

$$R^l = \sum_{\lambda=1}^3 V_{1\lambda} V_{\lambda 3}^{\dagger} D(-p_t, p_2, p_1, m_{\lambda}, m_{\bar{g}}, m_{\bar{g}}, m_{\bar{g}}), \quad R^m = R^l|_{V_{1\lambda} \rightarrow V_{2\lambda}}, \quad (\text{A8})$$

$$R^n = \sum_{\lambda=1}^3 V_{1\lambda} V_{\lambda 3}^{\dagger} D(p_1, p_2, -p_t, m_{\lambda}, m_{\lambda}, m_{\lambda}, m_{\bar{g}}), \quad R^o = R^n|_{V_{1\lambda} \rightarrow V_{2\lambda}}, \quad (\text{A9})$$

$$R^p = \sum_{\lambda=1}^3 V_{1\lambda} V_{\lambda 3}^{\dagger} D(-p_t, p_2, -p_c, m_{\lambda}, m_{\bar{g}}, m_{\bar{g}}, m_{\lambda}), \quad R^q = R^p|_{V_{1\lambda} \rightarrow V_{2\lambda}}, \quad (\text{A10})$$

where ρ and λ are squark indices in mass eigenstate, p_i is particle momentum, B, C and D are loop functions[27], and $F_{\lambda\rho}^Z$ and $F_{\lambda\rho}^h$ are interaction coefficients for $\tilde{q}_{\lambda}^* \tilde{q}_{\rho} Z$ and $\tilde{q}_{\lambda}^* \tilde{q}_{\rho} h$ interactions respectively, which are given by

$$F_{\lambda\rho}^Z = (1 - \frac{4}{3} s_W^2) \delta_{\rho\lambda} - V_{\lambda 2}^{\dagger} V_{2\rho} \quad (\text{A11})$$

$$F_{\lambda\rho}^h = -\frac{g}{m_W \sin \beta} \left(m_t^2 \cos \alpha (V_{\lambda 1}^{\dagger} V_{1\rho} + V_{\lambda 2}^{\dagger} V_{2\rho}) + \frac{m_t (A_t \cos \alpha + \mu \sin \alpha)}{2} (V_{\lambda 1}^{\dagger} V_{2\rho} + V_{\lambda 2}^{\dagger} V_{1\rho}) \right. \\ \left. + \frac{\delta_{LR} M_{Q_2} M_{U_3} \cos \alpha}{2} (V_{\lambda 3}^{\dagger} V_{2\rho} + V_{\lambda 2}^{\dagger} V_{3\rho}) \right). \quad (\text{A12})$$

Then after factoring out the common factor $\alpha_s/4\pi$, we obtain the expressions for Σ and Γ_s :

$$\Sigma(p) = -2C_F (\gamma^\mu R_\mu^a + m_{\bar{g}} R_0^b) P_L, \quad (\text{A13})$$

$$\Gamma_\mu^{\bar{t}cg} = \frac{1}{3} g_s T^a (2\gamma^\nu R_{\mu\nu}^c - 2m_{\bar{g}} R_\mu^d - (p_t + p_c)_\mu (\gamma^\nu R_\nu^c - m_{\bar{g}} R_0^d)) P_L + 3g_s T^a (\not{p}_t \gamma_\mu \not{p}'_c R_0^e - \not{p}'_t \gamma_\mu \gamma^\nu R_\nu^e - \gamma^\nu \gamma_\mu \not{p}'_c R_\nu^e + \gamma^\nu \gamma_\mu \gamma^\lambda R_{\nu\lambda}^e + m_{\bar{g}}^2 \gamma_\mu R_0^e - m_{\bar{g}} \gamma_\mu \not{p}'_c R_0^f + 2m_{\bar{g}} R_\mu^f - m_{\bar{g}} \not{p}'_t \gamma_\mu R_0^f) P_L, \quad (\text{A14})$$

$$\Gamma_\mu^{\bar{t}bcW} = \frac{g}{\sqrt{2}} C_F \gamma^\nu P_L (p_{b\mu} R_\nu^g - R_{\mu\nu}^g), \quad (\text{A15})$$

$$\Gamma_\mu^{\bar{t}cZ} = \frac{g}{c_W} C_F ((p_t + p_c)_\mu (\gamma^\nu R_\nu^h - m_{\bar{g}} R_0^i) - 2(\gamma^\nu R_{\mu\nu}^h - m_{\bar{g}} R_\mu^i)) P_L, \quad (\text{A16})$$

$$\Gamma_\mu^{\bar{t}c\gamma} = -2eQ_u C_F (2\gamma^\nu R_{\mu\nu}^c - 2m_{\bar{g}} R_\mu^d - (p_t + p_c)_\mu (\gamma^\nu R_\nu^c - m_{\bar{g}} R_0^d)) P_L, \quad (\text{A17})$$

$$\Gamma^{\bar{t}ch} = -2C_F (\gamma^\mu R_\mu^j - m_{\bar{g}} R_0^k) P_L, \quad (\text{A18})$$

where C_F is the quadratic Casimir operator of the fundamental representation of $SU(3)_C$.

For the box diagrams in Fig. 2, their results are given by

$$\begin{aligned} M_d = & -2\alpha_s^2 T^e T^a f^{deb} f^{cba} \varepsilon_\lambda^d(p_2) \varepsilon_\rho^c(p_1) \bar{u}_t (-m_{\bar{g}} m_t \gamma^\lambda (\not{p}'_t - \not{p}'_2) \gamma^\rho R_0^m \\ & + m_{\bar{g}} m_t \gamma^\lambda \gamma^\nu \gamma^\rho R_\nu^m + m_{\bar{g}} \gamma^\nu \gamma^\lambda (\not{p}'_t - \not{p}'_2) \gamma^\rho R_\nu^m - m_{\bar{g}} \gamma^\mu \gamma^\lambda \gamma^\nu \gamma^\rho R_{\mu\nu}^m \\ & - m_t \gamma^\lambda (\not{p}'_t - \not{p}'_2) \gamma^\rho \gamma^\nu R_\nu^l + m_t \gamma^\lambda \gamma^\mu \gamma^\rho \gamma^\nu R_{\mu\nu}^l + \gamma^\mu \gamma^\lambda (\not{p}'_t - \not{p}'_2) \gamma^\rho \gamma^\nu R_{\mu\nu}^l - \gamma^\mu \gamma^\lambda \gamma^\nu \gamma^\rho \gamma^\sigma R_{\mu\nu\sigma}^l \\ & + m_{\bar{g}}^2 m_t \gamma^\lambda \gamma^\rho R_0^l - m_{\bar{g}}^2 \gamma^\nu \gamma^\lambda \gamma^\rho R_\nu^l + m_{\bar{g}} m_t \gamma^\lambda \gamma^\rho \gamma^\nu R_\nu^m - m_{\bar{g}} \gamma^\mu \gamma^\lambda \gamma^\rho \gamma^\nu R_{\mu\nu}^m) P_L v_c, \end{aligned} \quad (\text{A19})$$

$$M_e = -8\alpha_s^2 T^a T^d T^c T^a \varepsilon_\lambda^d(p_2) \varepsilon_\rho^c(p_1) \bar{u}_t (\gamma^\nu R_{\nu\rho\lambda}^n + \gamma^\nu p_{1\lambda} R_{\nu\rho}^n + m_{\bar{g}} R_{\rho\lambda}^o + m_{\bar{g}} p_{1\lambda} R_\rho^o) P_L v_c, \quad (\text{A20})$$

$$\begin{aligned} M_f = & -4\alpha_s^2 T^a T^c T^b f^{dab} \varepsilon_\lambda^d(p_2) \varepsilon_\rho^c(p_1) \bar{u}_t (m_t \gamma^\lambda (\not{p}'_t - \not{p}'_2) R_\rho^p \\ & - m_t \gamma^\lambda \gamma^\nu R_{\nu\rho}^p - \gamma^\nu \gamma^\lambda (\not{p}'_t - \not{p}'_2) R_{\nu\rho}^p + \gamma^\mu \gamma^\lambda \gamma^\nu R_{\mu\nu\rho}^p - m_{\bar{g}} m_t \gamma^\lambda R_\rho^q \\ & + m_{\bar{g}} \gamma^\nu \gamma^\lambda R_{\rho\nu}^q - m_{\bar{g}} \gamma^\lambda (\not{p}'_t - \not{p}'_2) R_\rho^q + m_{\bar{g}} \gamma^\lambda \gamma^\nu R_{\rho\nu}^q + m_{\bar{g}}^2 \gamma^\lambda R_\rho^p) P_L v_c. \end{aligned} \quad (\text{A21})$$

- [1] For the FCNC top quark decays in the SM, see, G. Eilam, J. L. Hewett and A. Soni, Phys. Rev. D **44**, 1473 (1991); Erratum-ibid. D **59** 039901 (1999). B. Mele, S. Petrarca and A. Soddu, Phys. Lett. B **435**, 401 (1998); A. Cordero-Cid, J. M. Hernandez, G. Tavares-Velasco and J. J. Toscano, Phys. Rev. D **73**, 094005 (2006).
- [2] G. Eilam, M. Frank and I. Turan, Phys. Rev. D **73**, 053011 (2006).
- [3] C.-H. Chang, X.-Q. Li, J.-X. Wang and M.-Z. Yang, Phys. Lett. B **313**, 389 (1993) C.-S. Huang, X.-H. Wu and S.-H. Zhu, Phys. Lett. B **452**, 14 (1999).
- [4] For a recent review, see F. Larios, R. Martinez and M. A. Perez, Int. J. Mod. Phys. A **21**, 3473 (2006).
- [5] J. A. Aguilar-Saavedra, Acta Phys. Polon. B **35**, 2695 (2004).
- [6] J. A. Aguilar-Saavedra and T. Riemann, hep-ph/0102197; J. A. Aguilar-Saavedra, Phys. Lett. B **502**, 115(2001).
- [7] M. Paulini, hep-ex/9701019; J. Incandela (CDF), FERMILAB-CONF-95/237-E(1995); D. Gerdes, hep-ex/9706001; T. J. Lecompte (CDF), FERMILAB-CONF-96/021-E (1996); A. P. Heinson (D0), hep-ex/9605010.
- [8] For $t \rightarrow cV$ in the MSSM, see, C. S. Li, R. J. Oakes and J. M. Yang, Phys. Rev. D **49**, 293 (1994); G. Couture, C. Hamzaoui and H. Konig, Phys. Rev. D **52**, 1713 (1995); J. L. Lopez, D. V. Nanopoulos and R. Rangarajan, Phys. Rev. D **56**, 3100 (1997); G. M. de Divitiis, R. Petronzio and L. Silvestrini, Nucl. Phys. B **504**, 45 (1997); J. M. Yang, B.-L. Young and X. Zhang, Phys. Rev. D **58**, 055001 (1998); C. S. Li, L. L. Yang and L. G. Jin, Phys. Lett. B **599**, 92 (2004); D. Delepine and S. Khalil, Phys. Lett. B **599**, 62 (2004); M. Frank and I. Turan, Phys. Rev. D **74**, 073014 (2006).
- [9] For $t \rightarrow ch$ in the MSSM, see, J. M. Yang and C. S. Li, Phys. Rev. D **49**, 3412 (1994); J. Guasch and J. Sola, Nucl. Phys. B **562**, 3 (1999); G. Eilam, *et al.*, Phys. Lett. B **510**, 227 (2001); J. L. Diaz-Cruz, H.-J. He, C.-P. Yuan Phys. Lett. B **179**,530 (2002).
- [10] For top-charm associated productions in the MSSM at linear colliders, see, J. M. Yang, Annals Phys. **316**, 529 (2005); J. Cao, Z. Xiong and J. M. Yang, Nucl. Phys. B **651**, 87 (2003); C. S. Li, X. Zhang and S. H. Zhu, Phys. Rev. D **60**, 077702 (1999).
- [11] For top-charm associated productions in the MSSM at hadron colliders, see, J. J. Liu, C. S. Li, L. L. Yang and L. G. Jin, Nucl. Phys. B **705**, 3 (2005); J. Guasch, *et al.*, Nucl. Phys. Proc. Suppl. 157, 152 (2006) [hep-ph/0601218].
- [12] G. Eilam, M. Frank and I. Turan, Phys. Rev. D **74**, 035012 (2006).
- [13] For exotic top production processes in TC2 models, see, H. J. He and C. P. Yuan, Phys. Rev. Lett. **83**, 28(1999); G. Burdman, Phys. Rev. Lett. **83**,2888(1999); J. Cao, Z. Xiong and J. M. Yang, Phys. Rev. D **67**, 071701 (2003); C. Yue, *et*

- al. Phys. Lett. B* **496**, 93 (2000); C. Yue, *et al.*, *Phys. Lett. B* **525**, 301(2002); J. Cao, *et al. Phys. Rev. D* **70**, 114035 (2004); F. Larios and F. Penunuri, *J. Phys. G* **30**, 895(2004); J. Cao, *et al. Eur. Phys. Jour. C* **41**, 381 (2005).
- [14] For FCNC top quark decays in TC2 theory, see, X. L. Wang *et al.*, *Phys. Rev. D* **50**, 5781 (1994); C. Yue, *et al.*, *Phys. Rev. D* **64**, 095004 (2001); G. Lu, F. Yin, X. Wang and L. Wan, *Phys. Rev. D* **68**, 015002 (2003).
- [15] J. L. Diaz-Cruz, *et al. Phys. Rev. D* **41**, 891(1990); G. Eilam, *et. in Ref. [1]*; X.L. Wang *et al.*, *J. Phys. G* **20**, L91 (1994); *Commun. Theor. Phys.* **24**, 359 (1995); D. Atwood, L. Reina and A. Soni, *Phys. Rev. D* **53**, 1199 (1996); S. Bar-Shalom, *et al.*, *Phys. Rev. Lett.* **79**, 1217(1997); W. S. Hou, G.-L. Lin and C.-Y. Ma, *Phys. Rev. D* **56**, 7434(1997); S. Bejar, J. Guasch and J. Sola, *Nucl. Phys. B* **600**, 21 (2001); R. A. Diaz, R. Martinez, J.-A. Rodriguez, hep-ph/0103307; T. Han and J. Hewett, *Phys. Rev. D* **60**, 074015 (1999); F. del Aguila, J. A. Aguilar-Saavedra, R. Miquel, *Phys. Rev. Lett.* **82**, 1628 (1999); E. O. Iltan, *Phys. Rev. D* **65**, 075017 (2002); E. O. Iltan and I. Turan *Phys. Rev. D* **67**, 015004 (2003); J. A. Aguilar-Saavedra, B. M. Nobre, *Phys. Lett. B* **553**, 251 (2003); R. Gaitan, O. G. Miranda and L. G. Cabral-Rosetti, *Phys. Rev. D* **72**, 034018 (2005); A. Cordero-Cid, G. Tavares-Velasco and J. J. Toscano, *Phys. Rev. D* **72**, 057701 (2005); M. Frank and I. Turan, *Phys. Rev. D* **72**, 035008 (2005); A. Arhrib, K. Cheung, C. W. Chiang and T. C. Yuan, *Phys. Rev. D* **73**, 075015 (2006); H. Zhou, W. G. Ma, Y. Jiang, R. Y. Zhang and L. H. Wan, hep-ph/0107293; H. Zhou, W. G. Ma and R. Y. Zhang, hep-ph/0208170. P. M. Ferreira and R. Santos, *Phys. Rev. D* **73**, 054025 (2006); P. M. Ferreira and R. Santos, *Phys. Rev. D* **74**, 014006 (2006).
- [16] S. Dimopoulos and D. Sutter, *Nucl. Phys. B* **452**, 496 (1996); F. Gabbiani, *et al.*, *Nucl. Phys. B* **477**, 321 (1996); M. Misiak, S. Pokorski and J. Rosiek, hep-ph/9703442.
- [17] J. Cao, G. Eilam, K. Hikasa and J. M. Yang, *Phys. Rev. D* **74**, 031701 (2006).
- [18] J. Rosiek, hep-ph/9511250.
- [19] T. Besmer, C. Greub, T. Hurth, *Nucl. Phys. B* **609**, 359 (2001); F. Borzumati, *et al.*, *Phys. Rev. D* **62**, 075005(2000).
- [20] M. Ciuchini, E. Franco, A. Masiero and L. Silvestrini, hep-ph/0307194; P. Ball, S. Khalil and E. Kou, *Phys. Rev. D* **69**, 115011 (2004); M. Ciuchini and L. Silvestrini, *Phys. Rev. Lett.* **97**, 021803 (2006).
- [21] J. Hewett *et al.*, hep-ph/0503261.
- [22] L. J. Hall, V. A. Kostelecky and S. Raby, *Nucl. Phys. B* **267**, 415 (1986); F. Gabbiani and A. Masiero, *Nucl. Phys. B* **322**, 235 (1989); J. S. Hagelin, S. Kelley and T. Tanaka, *Nucl. Phys. B* **415**, 293 (1994).
- [23] A.H. Chamseddine, R. Arnowitt and P. Nath, *Phys. Rev. Lett.* **49**, 970 (1982); R. Barbieri, S. Ferrara and C.A. Savoy, *Phys. Lett. B* **119**, 343 (1982); L. Hall, J. Lykken and S. Weinberg, *Phys. Rev. D* **27**, 2359 (1983); H. P. Nilles, *Phys. Report* **110**, 1 (1984); M. Drees and S. P. Martin, hep-ph/9504324.
- [24] N. Arkani-Hamed, J. March-Russell and H. Murayama, *Nucl. Phys. B* **509**, 3(1998); H. Murayama, *Phys. Rev. Lett.* **79**, 18 (1997); K.-I. Izawa, Y. Nomura, K. Tobe and T. Yanagida, *Phys. Rev. D* **56**, 2886(1997); M.A. Luty, *Phys. Lett. B* **414**, 71(1997).
- [25] K. Hikasa and M. Kobayashi, *Phys. Rev. D* **36**, 724 (1987); M. J. Duncan, *Nucl. Phys. B* **221**, 285 (1983).
- [26] T. Hahn and M. Perez-Victoria, *Comput. Phys. Commun.* **118**, 153 (1999); T. Hahn, *Nucl. Phys. Proc. Suppl.* **135**, 333 (2004).
- [27] G. Passarino and M. J. G. Veltman, *Nucl. Phys. B* **160**, 151 (1979); G. 't Hooft and M. J. G. Veltman, *Nucl. Phys. B* **153**, 365 (1979).
- [28] Vernon D. Barger and R.J.N. Phillips, *Collider Physics*, Addison-Wesley (1987).
- [29] W. M. Yao *et al.* [Particle Data Group], *J. Phys. G* **33**, 1 (2006).
- [30] M. Carena, S. Heinmeyer, C. E. M. Wagner, G. Weiglein, hep-ph/9912223.
- [31] S. Heinmeyer, *et al.*, *Eur. Phys. Jour. C* **37**, 481 (2004).
- [32] J. Pumplin, A. Belyaev, J. Huston, D. Stump and W. K. Tung, *JHEP* **0602**, 032 (2006).
- [33] M. Hosch, K. Whisnant and B. L. Young, *Phys. Rev. D* **56**, 5725 (1997).
- [34] T. Stelzer, Z. Sullivan and S. Willenbrock, *Phys. Rev. D* **58**, 094021 (1998).
- [35] T. Han, M. Hosch, K. Whisnant, B. L. Young and X. Zhang, *Phys. Rev. D* **58**, 073008 (1998).
- [36] K. Inoue, A. Kakuto, H. Komatsu and S. Takeshita, *Prog. Theor. Phys.* **67**, 1889 (1982); *Prog. Theor. Phys.* **68**, 927 (1982) [Erratum-ibid. **70**, 330 (1983)]; *Prog. Theor. Phys.* **71**, 413 (1984).
- [37] S. Heinmeyer, W. Hollik, D. Stockinger, A. M. Weber and G. Weiglein, *JHEP* **0608**, 052 (2006).
- [38] R. Barbieri and G. F. Giudice, *Phys. Lett. B* **309**, 86 (1993).
- [39] E. Gabrielli, K. Huitu and S. Khalil, *Nucl. Phys. B* **710**, 139 (2005); Z. J. Xiao, F. G. Li and W. J. Zou, hep-ph/0603120.
- [40] HFAG Group, <http://www.slac.stanford.edu/xorg/hfag>.
- [41] P. Gambino and M. Misiak, *Nucl. Phys. B* **611**, 338(2001); A.J.Buras, A. Czarnecki, M. Misiak, and J. Urban, *Nucl. Phys. B* **631**, 219 (2002); C. Bobeth, P. Gambino, M. Gorbahn, and U. Haisch, *JHEP* **04**, 071 (2004) 071; A. Ghinculov, T. Hurth, G. Isidori, and Y.P. Yao, *Nucl. Phys. B* **685**, 351(2004).
- [42] P. Gambino, U. Haisch and M. Misiak, *Phys. Rev. Lett.* **94**, 061803(2005).
- [43] V. M. Abazov *et al.* [D0 Collaboration], *Phys. Rev. Lett.* **97**, 021802 (2006).
- [44] M. Bona *et al.* [UTfit Collaboration], *JHEP* **0507**, 028 (2005).
- [45] J. Charles *et al.* [CKMfitter Group], *Eur. Phys. Jour. C* **41**, 1 (2005).
- [46] M. Endo and S. Mishima, *Phys. Lett. B* **640**, 205 (2006).
- [47] See, e.g., P. Chankowski, *et al.*, *Nucl. Phys. B* **417**, 101 (1994); D. Garcia and J. Solà, *Mod. Phys. Lett. A* **9**, 211 (1994).
- [48] The LEP Collaborations, hep-ex/0509008.
- [49] A. Dabelstein, *Z. Phys. C* **67**, 495 (1995).
- [50] H.E. Haber, R. Hempfling, *Phys. Rev. Lett.* **66**, 1815 (1991); Y. Okada, M. Yamaguchi, T. Yanagida, *Prog. Theor. Phys.* **85**, 1 (1991); *Phys. Lett. B* **262**,54(1991); J. Ellis, G. Ridolfi, F. Zwirner, *Phys. Lett. B* **257**, 83 (1991); *Phys. Lett. B*

- 262**, 477 (1991); J. R. Espinosa and R. J. Zhang, JHEP **0003** (2000) 026.
- [51] S. Heinemeyer, Int. J. Mod. Phys. A **21**, 2659 (2006); T. Hahn, W. Hollik, S. Heinemeyer and G. Weiglein, hep-ph/0507009.
- [52] M. Carena, *et al.*, Eur. Phys. Jour. C **26**, 601 (2003).
- [53] J. A. Aguilar-Saavedra and G. C. Branco, Phys. Lett. B **495**, 347 (2000).
- [54] T. Han, R. D. Peccei and X. Zhang, Nucl. Phys. B **454**, 527 (1995).
- [55] L. Chikovani and T. Djobava, hep-ex/0205016.
- [56] M. Beneke *et al.*, hep-ph/0003033.
- [57] F. del Aguila and J. A. Aguilar-Saavedra, Nucl. Phys. B **576**, 56 (2000).
- [58] T. Han, K. Whisnant, B. L. Young and X. Zhang, Phys. Lett. B **385**, 311 (1996).
- [59] T. Han, K. Whisnant, B. L. Young and X. Zhang, Phys. Rev. D **55**, 7241 (1997).
- [60] Another advantage of allowing the parameters to vary within a large range is that, for most of the processes considered in this paper, the dependence of their rates on δ_{RL} and δ_{RR} is similar to that on δ_{LR} and δ_{LL} . But the indirect constraints on them are quite different: while the indirect constraints on δ_{LL} and δ_{LR} may be quite stringent, the limits on δ_{RL} and δ_{RR} are rather weak [17]. Therefore, the allowed range of δ_{RL} and δ_{RR} is much larger than δ_{LL} and δ_{LR} .
- [61] There is a typo in Eq. (15) of Ref. [17]: δ_{LL} and δ_{LR} were required to vary between 0 and 2 rather than between 0 and 1. We checked that allowing δ parameters to be larger than 2 does not affect the results in Table I, but more samples are needed to get the results in Table I. In our scan, we required $\delta_{RL}^d = \delta_{RR}^d = 0$ and $\delta_{LL}, \delta_{LR} > 0$. Relaxing these requirements does not change our results but lowers the efficiency to search for the maximal predictions in a certain number of samples. In our scan, we also found that our results are not sensitive to the values of M_{D_i} , M_{U_1} , M_{Q_1} and A_b .